

Review

Micro-Vibration Analysis, Suppression, and Isolation of Spacecraft Flywheel Rotor Systems: A Review

Qinkai Han ^{1,*} , Shuai Gao ² and Fulei Chu ¹ 

¹ The State Key Laboratory of Tribology, Department of Mechanical Engineering, Tsinghua University, Beijing 100084, China; chuf@mail.tsinghua.edu.cn

² State Key Laboratory of Mechanical Transmission for Advanced Equipment, College of Mechanical Engineering, Chongqing University, Chongqing 400044, China; shuai.gao@cqu.edu.cn

* Correspondence: hanqinkai@mail.tsinghua.edu.cn; Tel.: +86-10-62788308

Abstract: In this paper, the main excitation sources of micro vibration of spacecraft flywheel rotor systems (SFRSs) are briefly described, and then the research progress is systematically reviewed from four perspectives, including modeling methods, suppression means, vibration isolation techniques, and ground simulation tests. Finally, the existing problems of current research and the direction of further research are given to better serve the micro-vibration prediction and sensitivity analysis of existing models, and provide reference points for the micro-vibration suppression and isolation of the next generation of high-precision spacecraft.

Keywords: spacecraft flywheel rotor systems; micro-vibration modeling; vibration suppression; vibration isolation; dynamic tests on the ground

1. Introduction

High precision earth observation satellites can obtain high-quality remote sensing images, which can greatly assist the development requirements of economy, society, and science and technology, and have become the focus of competitive development among the world's aerospace powers [1,2]. In addition to earth observation, high-precision spacecraft also play an important role in various aerospace applications, such as deep space physical exploration, astronomical observation, and satellite laser communication. Therefore, high-precision spacecraft are an important focus for the development of the world aerospace industry [3–5].

As an inertial actuator, a spacecraft flywheel rotor system (SFRS) is applied for spacecraft attitude control and large-angle rotation maneuver [6]. According to whether the rotation axis of the rotor is fixed or not, SFRSs are divided into two types: the fixed-shaft type and the non-fixed-shaft type. As shown in Figure 1a, both reaction wheel assemblies (RWA) and momentum wheel assemblies (MWA) belong to the fixed-shaft type SFRS. By adjusting the rotation speed of the rotor, a reaction torque is obtained, and the momentum moment is exchanged with the spacecraft to realize attitude control. The RWA usually has zero nominal speed, and the speed range is mostly within ± 4000 rev/min, while the MWA generally has a higher nominal speed (3000–6000 rev/min) and a greater axial moment of inertia [7]. The non-fixed-shaft type SFRS (see Figure 1b) mainly refers to the control moment gyroscope (CMG). A flywheel rotor is generally suspended by a gimbal, and the precession of the rotor is induced by the gimbal's rotation to produce a reaction gyro moment, which is used for spacecraft attitude control. The rotor speed of the CMG is constant, but the rated speed is relatively high, generally up to 4000–9000 rev/min [7].

The high-speed SFRS is the main excitation source of micro vibration for the in-orbit spacecraft, and its micro-vibration characteristics are the key factors affecting the attitude stability and pointing accuracy of the platform [8–11]. The frequency range of micro-vibration disturbance of the SFRS is generally wide (about 1–1000 Hz), and the influence of



Citation: Han, Q.; Gao, S.; Chu, F. Micro-Vibration Analysis, Suppression, and Isolation of Spacecraft Flywheel Rotor Systems: A Review. *Vibration* **2024**, *7*, 229–263. <https://doi.org/10.3390/vibration7010013>

Academic Editor: Giuseppe Quaranta

Received: 27 January 2024

Revised: 1 March 2024

Accepted: 5 March 2024

Published: 11 March 2024



Copyright: © 2024 by the authors. Licensee MDPI, Basel, Switzerland. This article is an open access article distributed under the terms and conditions of the Creative Commons Attribution (CC BY) license (<https://creativecommons.org/licenses/by/4.0/>).

disturbance in the range of 10–200 Hz is the most prominent. The frequency range of this disturbance is far beyond the bandwidth capability of the attitude and orbit control system (AOCS), and could not be effectively suppressed by the AOCS [12]. By adding a damping dissipative structure and vibration isolator, the transmission path of micro vibration of the SFRS can be effectively isolated, which is an effective method for micro-vibration suppression of conventional spacecraft [13].

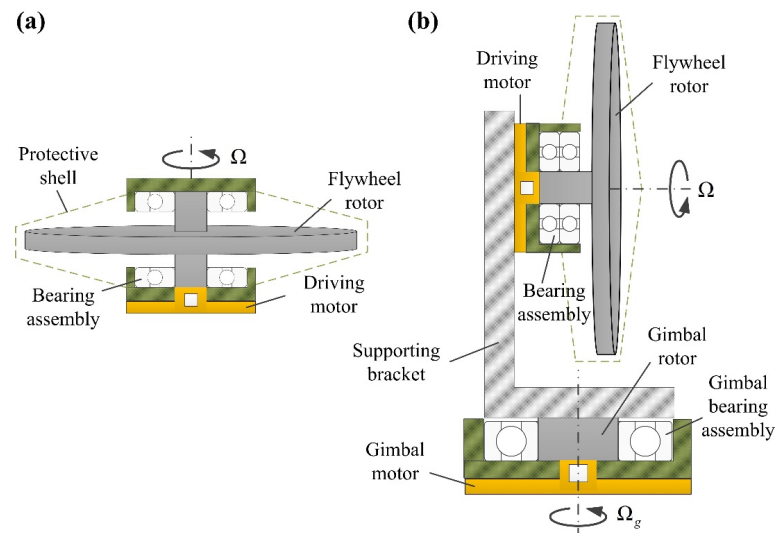


Figure 1. Schematic pictures for (a) fixed-shaft type SFRS and (b) non-fixed-shaft type SFRS.

Compared with conventional spacecraft, the high-precision spacecraft represented by high-resolution satellites, laser communication satellites, and space telescopes require “super stable” attitude and “super precision” pointing [14–17]. For instance, the pointing stability of the Hubble space telescope (HST) is required to be less than 0.007 arc sec within 24 h; the space interference mission (SIM) and advanced technology large space telescope (ATLAST) require the pointing stability to reach 0.0016 arc sec, and the vibration interference to the platform is required to be below 10^{-6} g level. For a laser beam with a diameter of 100 mm emitted by a laser communication satellite, a jitter of 0.001 radian at a distance of 500 km will reduce the beam intensity received by the receiver by 100 times. For Earth–Moon laser communication, the distance between the transmitter and the receiver is measured in tens of thousands of kilometers. For deep space communication, it is expected to reach 0.1–40 astronomical units. The slightest jitter of the platform will cause the direction of the laser beam to widely diverge!

Conventional micro-vibration suppression methods, such as the damping dissipative structure and vibration isolator, can only solve the symptoms but not the root cause, which is difficult to meet due to the extremely high requirements of high-precision spacecraft on the micro vibration of the SFRS. Mastering the micro-vibration mechanism, conducting sensitivity analysis and transmission path research, and then designing targeted suppression and isolation measures, are the only way to solve the micro vibration problem of the SFRS in high-precision spacecraft. In the past 20 years, many scholars have conducted systematic and comprehensive research on the micro vibration of SFRSs. In this paper, the main excitation sources of micro vibration of SFRSs are briefly described, and then the research progress is systematically reviewed from four perspectives, including the modeling methods, suppression means, vibration isolation techniques, and ground simulation tests. Finally, the existing problems of current research and the direction of further research are suggested to better serve the micro-vibration prediction and sensitivity analysis of the existing models, and provide reference for micro-vibration suppression and isolation in the next generation of high-precision spacecraft.

2. Disturbance Sources of Micro Vibration of SFRSs

As shown in Figure 1a, the fixed-shaft type SFRS is mainly composed of a flywheel, a bearing assembly, a drive motor, a protective shell and a support base. The non-fixed-shaft type SFRS is usually composed of a high-speed rotor, a gimbal system and a gyro house. The structure of the high-speed rotor is similar to that of the fixed-shaft type SFRS. The difference is that the shell is connected with a gimbal, as shown in Figure 1b. The gimbal system is composed of the support bearings, a driving motor, and the mounting bracket. The flywheel and bearing systems are the core components of the SFRS. The high-speed flywheel has the structural characteristics of light weight, great moment of inertia, and good rigidity. According to the support principle, the bearing system includes two categories: mechanical bearings and magnetic bearings. Presently, most of the SFRSs in service are supported by mechanical rolling bearings.

Since the 1990s, in-depth research has been conducted on the basic causes of micro-vibration disturbance of the SFRS [18,19]. Regardless of the aerospace application background, the SFRS has a similar structure to that of rotor systems on the ground. In general, there are three kinds of excitation sources which affect the micro vibration of the SFRS: mechanical disturbance, electromagnetic disturbance, and structural disturbance, as shown in Figure 2. Mechanical disturbance includes rotor imbalance, irrational characteristics of rolling bearings, flywheel rotor rub impact, etc. Electromagnetic disturbance includes torque ripple of the driving motor, imbalanced magnetic pull force, etc. Structural disturbance includes the structural vibration of the flywheel, the flexibility of the support structure, and the clearance effect. Micro vibration appears under the above multi-source excitations. After transmission and amplification by the internal structure, the SFRS produces significant micro vibration disturbances when it outputs the required control torque to the spacecraft. It will not only seriously affect the normal operation of the payload, but also cause the flywheel rotor to work abnormally or even fail. Therefore, effective identification and accurate modeling of micro-vibration excitation sources are the premise of micro-vibration analysis of the SFRS. The following describes the specific characteristics of the above three kinds of excitation sources.

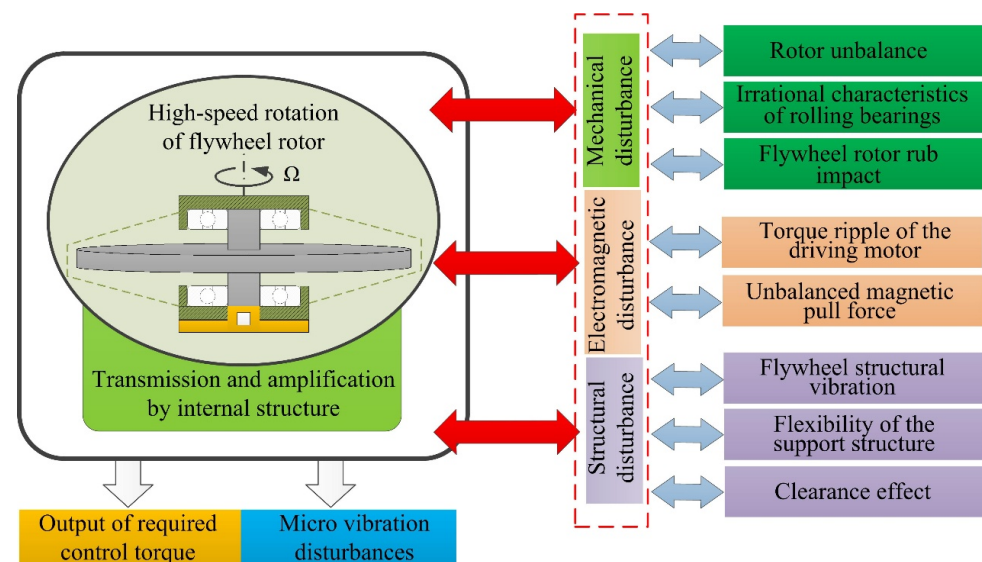


Figure 2. Disturbance sources of micro vibration of the SFRS.

2.1. Mechanical Disturbance

The mechanical disturbances caused by rotor imbalance, non-ideal characteristics of rolling bearings, and rotor rub impact, are the main excitation sources of the SFRS. In the processing and assembly of the rotor, there are inevitable error factors, which make the rotor imbalanced. Although the rotor will be dynamically balanced before space

application, the imbalanced mass cannot be completely eliminated [20]. Therefore, the imbalance disturbance excitation appears along with the high-speed rotation of the rotor. Rotor imbalance can be divided into static imbalance and dynamic imbalance. A deviation between the mass center of the rotor and rotating shaft induces a static imbalance, and excitation forces are generated in the process of rotor rotation. Dynamic imbalance is caused by a deviation between the inertial principle axis and the rotating shaft, and excitation torques are generated in the process of rotor rotation [21].

The rolling bearing in the SFRS mainly plays a supporting role, and the disturbance introduced by the rotor is transmitted outward through the bearings. Usually, the components of rolling bearings, including ball, inner ring, outer ring, and cage (or retainer), have non-ideal characteristics, such as surface waviness, clearance, friction, and so on. Waviness is an important structural feature of rolling bearings. It is a geometric defect on the surface of bearing components, which is a harmonic waveform distribution. When bearing components are finished on a grinder, the vibration of the machine tool will leave uneven geometric features on their surfaces, which is the cause of waviness [22]. In modern bearing manufacturing, the amplitude of bearing waviness can be controlled at the micro-meter level. However, during the working process of the bearing, the waviness can still cause prominent vibration problems [23–25]. The results show that raceway waviness can cause frequency division and frequency-doubling vibration characterized by the rolling element passing frequency [26–31]. As for the friction characteristic, it is due to machining accuracy. Even after lubrication design, friction still exists between the ball and raceways [32]. Especially for the CMG, bearing friction is one of the most important disturbance factors in its low-speed gimbal system [33].

When the vibration amplitude exceeds the structural gap, intermittent or continuous collision and friction occur between the flywheel rotor and the fixed structure, which is called rotor rub impact [34]. Uneven mass distribution of the flywheel, bending of the rotor structure, shaft misalignment, and insufficient gap caused by changes of environmental temperature may cause such a phenomenon. Generally, rotor rub impact can be divided into four stages: (1) normal operation without rub impact; (2) initial stage of rub impact; (3) frictional process stage; (4) frictional separation stage. These four stages occur alternately in actual rotor rub impact, resulting in complex nonlinear phenomena. In this regard, relevant scholars have carried out continuous theoretical and experimental research [35–39].

2.2. Electromagnetic Disturbance

Most SFRSs use a brushless DC motor as the driving component. Due to the current pulsation and regulation in the control system, an obvious ripple phenomenon exists in the motor output torque, which causes flywheel speed instability and micro vibration problems [40]. In addition to the torque ripple, uneven electromagnetic force at the radial points of the rotor, namely the imbalanced magnetic pull, is also one of the main factors causing vibration of the SFRS [41]. The causes of imbalanced magnetic pull include mechanical and electromagnetic aspects. The mechanical aspect is air gap eccentricity due to misalignment between the stator and rotor, which includes static eccentricity, dynamic eccentricity, and hybrid eccentricity [42]. Height difference between the bearings on both sides of the supporting rotor shaft, inclination of the rotating shaft, and wear of the bearing will cause differences in the air gap of the motor along the axial direction, which is known as slant eccentricity [43]. The electromagnetic aspect includes uneven magnetization of materials, improper winding, or short circuit. For the electromagnetic disturbance caused by imbalanced magnetic pull, relevant scholars have carried out systematic modeling and analysis work [44–48].

2.3. Structural Disturbance

Although the structural stiffness of the components of the SFRS is relatively high, there is still a certain flexibility, which comes from the rotor, bearing system, supporting

shell, etc. The structural flexibility has an important impact on the disturbance output of the SFRS. The elastic modes of the SFRS include three types [49]: (1) axial translation mode, (2) radial rocking (or overturning) mode, and (3) radial translation mode. Under the action of excitations, the components will vibrate elastically due to structural flexibility. Especially for an excitation frequency close to the natural frequency of the SFRS, the output disturbance will be amplified. For example, the transient torque ripple of the driving motor may excite the elastic mode of the SFRS. The bearing system has nonlinear contact stiffness, which results in obvious frequency doubling phenomena of disturbance output spectra [50]. Owing to the discontinuous support of rolling elements, time-varying stiffness excitation is caused. The variation frequency of the stiffness is related to the number of balls and the rotational speed. When the stiffness frequency equals the natural frequency of the component structure, it will also cause large disturbance output and even structural instability [51,52].

3. Micro Vibration Models of SFRSs

Considering the complex structures and various disturbance sources, effective modeling of the micro-vibration characteristics of the SFRS is one of the focuses of current research. With reference to the types of micro-vibration models, the existing research mainly includes the empirical model, analytical model, and hybrid model. The relevant progress will be reviewed below.

3.1. Empirical Models

An empirical model is developed by statistical analysis of experimental results and data fitting. Harsha [53] and Masterson et al. [54] first proposed such a model to predict the influence of micro vibrations produced by the SFRS on the HST. The basic idea of the empirical model is to assume that the disturbance of the SFRS is a series of discrete harmonics with the amplitudes proportional to the square of the rotor speed Ω . The specific form is presented as follows

$$f(t) = \sum_{i=1}^n C_i \Omega^2 \sin(2\pi h_i \Omega t + \alpha_i) \quad (1)$$

where C_i , h_i , α_i represent the amplitude coefficient, order, and phase of the i th order of harmonics, respectively. Since the final output of the SFRS disturbance is measured experimentally, the empirical model (Equation (1)) can simultaneously reflect the harmonic disturbance output and broadband noise of the SFRS. The core problem of empirical models is to accurately identify the model parameters. The traditional amplitude spectra method has the problem of energy leakage due to signal truncation in the time domain, which makes the recognition accuracy of the amplitude coefficients very low. In order to overcome this problem, Zhao et al. [55] proposed an energy compensation method, which can significantly improve the identification accuracy of the empirical model parameters by improving the local energy at the broadband resonant frequency. On this basis, they applied the empirical model to the structural dynamic analysis of a spacecraft [56]. Recently, Yin et al. [57] proposed a signal denoising method based on the singular value decomposition and Akaike information criterion, and applied it to effectively extract the weak amplitude parameters of micro-vibration harmonics of an RWA. Shields et al. [58] adopted the empirical model to model the disturbing forces and moments of an RWA for a micro-cubic satellite. Analysis of the ASTERIA mission showed that the RWA produces a jitter of about 0.1 arc sec (RMS value) on the tip/tilt axis of the payload.

The interaction between various harmonics and structural modes of the SFRS is neglected, and thus the empirical model may underestimate the micro vibration disturbance in some speed ranges. Based on dynamic mass measurement technology, Elias and Miller [59] proposed a coupling empirical model, which considered the dynamic mass coupling effect of internal structural components of the RWA. Experimental results showed that [60] when there is a strong coupling between the gyroscopic effect and micro-vibration harmonics of

the rotating RWA, the proposed coupling empirical model provides better results compared with the decoupling model. Shigemune and Yoshiaki [61] developed an empirical model observer, which can detect low-frequency vibration disturbances. The dynamic simulation results showed that the observer can reflect the influence of defects such as deviation, size error, and mass imbalance on the micro-vibration disturbance of the SFRS. Recently, Xia et al. [62] introduced an amplification factor coefficient, which enables the empirical model to accurately consider the interaction between the SFRS structural mode and disturbance harmonics. The results showed that the average error of the improved empirical model can be controlled within 5%. Using the dynamic mass test method and quantitative impedance theory, the improved empirical model can consider the influence of installation stiffness on the disturbance test results.

Modal gain uncertainty refers to the fact that magnitudes of most of the high frequency modes were not validated by test data. To protect against modal gain uncertainty, the jitter analysis required a 100% margin on the current best estimate jitter when compared to the allocated requirements. Uncertainty also exists in modal frequency. Only the frequencies of primary (i.e., high modal mass) modes could be matched to the test data, and the frequencies of other modes could be in error by 5% to 10% or more. In order to estimate the impact of modal frequency uncertainty on the analysis results, the frequency sensitivity analyses should be performed by either varying the FEM modal frequencies or the input disturbance frequencies, by $\pm 10\%$. The worst-case result from the frequency sweep studies was reported to guard against frequency uncertainty.

For the gimbal rotor system of CMG, Huang et al. [63] established a high-order extended harmonic disturbance observer (EHDO) model which can describe the disturbance dynamics. Compared with the traditional extended disturbance observer, the EHDO can estimate multiple disturbances with higher accuracy in lower bandwidth. Based on this model, they also indirectly measured the dynamic imbalance excitation of the CMG rotor [64].

3.2. Analytical Models

Based on the working principle and structural dynamic characteristics of the SFRS, the analytical model is established by theoretical derivation, and its specific form is presented as follows

$$M\ddot{x} + (G + C)\dot{x} + Kx = F(t) \quad (2)$$

where x denotes the vector of degrees of freedom (DoFs) of the SFRS, which can be described as a five DoFs system which consists of one single DoF in axial translation, two DoFs in each radial (or in-plane) translations, and two DoFs in each radial (or out-of-plane) rotations. M , G , C , K are the mass, gyroscopic, damping, and stiffness matrices of the system, respectively. The damping effects mainly arise from the bearings, interface plates, and isolators. Due to low damping in the SFRS, however, damped natural frequencies do not significantly differ from the undamped ones. $F(t)$ is the external excitation vector considering the mechanical, electromagnetic, and structural disturbances of the SFRS. Both sub- and higher harmonics, and the broadband noise excitations, can be superimposed to fundamental harmonics in $F(t)$. Parameters for harmonic excitation modelling in Equation (1) include the amplitude coefficients, and harmonic number considered in each DoF. Broadband excitations, on the other hand, can be expressed as random noise components at this stage. Obviously, Equation (2) shows a set of coupled second order differential equations.

Considering the residual imbalance of the SFRS as the only disturbance source, Bialke [19] and Masterson [65] firstly established the analytical model of RWA. The model ignored the axial and torsional degrees of freedom, and was essentially a four degrees-of-freedom rotor model. As the two translational and two rocking degrees of freedom of the SFRS were considered, thus the model could well reflect the influence of the internal dynamic behavior of the SFRS on the micro-vibration output, including the dynamic amplification effect on the disturbance and gyroscopic effect of the high speed rotor. Li et al. [66]

and Deng et al. [67] both studied the natural characteristics and whirl response of an SFRS system based on the four degrees-of-freedom analytical model.

By taking into account the axial degree of freedom, Zhang et al. [68,69] proposed a five degrees-of-freedom analytical model, to analyze the micro-vibration response of a soft suspension-supported MWA system. The influence of mass imbalance, broadband noise, and dynamic coupling between the installation foundation and flywheel were theoretically predicted. The results indicated that the designed soft suspension system can effectively suppress the high-frequency micro-vibration response. Zhang et al. [70,71] also carried out numerical analysis and experimental research on the system. The results demonstrated that the gyroscopic effect has a significant effect on the micro-vibration response of the system under the acceleration state, and should be considered in the analytical model. The consistency between the model predicted and the measured results could be significantly improved by using the dynamic mass correction coefficient [72]. In addition, based on the analytical model, they also established a new method to obtain the dynamic mass of the RWA in its operating speed range [73]. Thus, an alternative measurement program is developed, which can achieve good estimation in a wide frequency range by relatively simple dynamic tests. For the SFRS supported by a two degrees-of-freedom radial magnetic bearing and three degrees-of-freedom axial magnetic bearing, Peng et al. [74] established a five degrees-of-freedom analytical model, and verified the correctness of the proposed model through micro-vibration test. Luo et al. [75] introduced the five degrees-of-freedom analytical model into the dynamic characteristic simulation of a multi-flywheel-shaft-isolation coupling system. The results showed that the mass and inertia characteristics of the system could be accurately reflected, and the gyroscopic effect of the multi-flywheel system makes the structural modes of the system strongly coupled. Based on the nonlinear contact force and the modified Coulomb friction model, Wan et al. [76] proposed an analytical model for the clearance between the flywheel rotor and the rolling bearing. Through the simulation analysis of the five degrees-of-freedom analytical model, the influence of clearance length, angular driving velocity, and friction coefficient on the micro-vibration characteristics of the MWA was studied.

Torque ripple and imbalanced magnetic pull would cause torsional and radial vibrations of the SFRS. Using a single degree of freedom torsional vibration model, Chou and Liaw [77] developed a robust dynamic control method for an RWA driven by the SPMSM, and realized flywheel health state monitoring through friction torque estimation. Based on the first principle, and considering the pure torsional degree of freedom of flywheel, Alcorn et al. [78] established a full coupled model of an SFRS, and analyzed the influence of static and dynamic imbalance on spacecraft jitter response. Based on the fully coupled model, Wang et al. [79] proposed an adaptive momentum distribution jitter-control method. The results demonstrated that the control method can significantly reduce the influence of reaction wheel jitter, and improve the spacecraft control accuracy by an order of magnitude. By introducing the torsional degree of freedom into the classical four degrees-of-freedom analytical model, Aghalari and Shahravi [80] proposed a five degrees-of-freedom analytical model of the RWA driven by a BLDC. The dynamic eccentric magnetic pull force and gyroscopic effect, dry friction (relative small sliding), and bearing friction of the shaft joint were considered. The model can reveal the micro-vibration characteristics of the RWA under the acceleration state.

Narayan, Nair and Ghosal [81] proposed a more general six degrees-of-freedom model to study the dynamic coupling between the SFRS and its bracket. After dynamic simulation and vibration test, it was observed that the gyroscopic force produced by the rotor is significant, which should be considered in the design of the mounting bracket. Wei et al. [82] regarded the SFRS and vibration isolation platform with six degrees of freedom in space as an integral system, and established an equivalent dynamic analytical model. It was verified by eigenvalue and frequency response analysis. By analyzing the vibration isolation performance of the platform under synchronous and high-order harmonic disturbances induced by the SFRS, it was demonstrated that the position of critical speed of the flywheel

has great influence on the effective speed range and disturbance attenuation rate of the passive platform. Preda et al. [83] introduced the six degrees-of-freedom analytical model into the modeling of the RWA/active vibration isolation platform/spacecraft coupling system. Considering the flexibility of the bearing isolator, the gyroscopic effect of the rotor, the dynamic characteristics of the actuator, and the closed-loop hysteresis, a robust control strategy was proposed to realize active attenuation performance in a wide speed range. By reasonably adjusting the parameters of the active controller, the robustness and performance can be relatively balanced [84].

Most of the above analytical models focus on the modeling of mechanical disturbance (mainly mass imbalance), electromagnetic disturbance, structural disturbance (including support structure flexibility, vibration isolation platform coupling, etc.), and their influences on the micro vibration of SFRSs [19,65–84]. The core supporting component, angular contact rolling bearings, plays a decisive role in the performance, operation reliability, and service life of the SFRS system. Among most of the existing analytical models, the rolling bearing is usually simplified by a linear spring-damper system [19,65–84]. The Hertzian contact, radial/axial clearance, surface waviness, and preloading conditions would have a significant impact on the dynamic characteristics of rolling bearings, and then affect the micro-vibration characteristics of the SFRS. Evidently, this linear treatment of the rolling bearing is too ideal. Zhou et al. [85] introduced the high frequency interference characteristics and nonlinear stiffness of rolling bearings into the analytical model of the SFRS. Simulation results showed that when the bearing disturbance frequency is close to the rotor translation mode at high speed, the dynamic amplification effect is even higher than the micro-vibration response caused by the mass imbalance. In the model, the nonlinear stiffness caused by surface waviness and the high frequency interference characteristics of bearings were given by an empirical formula, which might reduce the accuracy of the model.

The micro-vibration response of the SFRS is strongly coupled with the contact deformations between the rolling element and inner/outer raceways. How to accurately describe such a relationship is the key to establish the analytical model of the SFRS. Most current research mainly adopts the equivalent linear algorithm and the displacement coordination algorithm to decouple the relationship. Although the calculation efficiency is improved, the model accuracy is reduced. Based on the kinematic analysis of rolling bearings [31,86], a research team led by Han and Chu proposed a nonlinear iterative algorithm for load distribution of angular contact rolling bearings [87], which efficiently solved the nonlinear algebraic equations describing the geometric relationship, force balance relationship, elastohydrodynamic lubrication condition, and Hertzian contact of rolling bearings. The proposed nonlinear iterative algorithm accurately described the strong coupling relationship between the micro contact deformation and the dynamic response of the SFRS. Taking a high-speed rotor supported by an aerospace 7004C type angular contact rolling bearing as an example, the micro vibration response obtained by three algorithms was compared [87]. The results showed that the dynamic response obtained by the nonlinear iterative algorithm is closest to the measured results, while the other two algorithms overestimate (for the displacement coordination algorithm) or underestimate (for the equivalent linear algorithm) the micro-vibration response of the system. Combined with the nonlinear iterative algorithm of angular contact rolling bearings, Wang and Han [88] established a rigid-flexible coupling analytical model to accurately predict the micro-vibration response of an SFRS. The influences of bearing geometric parameters, preload, rotating speed, lubrication conditions, and other factors on the micro-vibration response were analyzed and discussed. The micro vibration characteristics of the 350 type MWA were studied. Comparisons with the measured results showed that the proposed analytical model is reliable [88]: the rotating speed and its multiples, parametric excitation frequencies caused by bearing stiffness variation, and characteristic frequencies caused by raceway surface waviness, were accurately predicted, with frequency error less than 5%. Except for the individual frequencies, the amplitude prediction error of key frequencies

is within 30%. Based on the analytical model and frequency sweep analysis, it was found that there are forward and backward whirling frequencies in the micro-vibration response, which reflects the strong coupling effect between the flywheel structure and gyroscopic effect. Among some speed ranges, for instance, the excitation frequency is close to the natural frequency, and the amplitude mutation and jump appear in the micro-vibration response, which is consistent with the test results.

The above analytical model is mainly aimed at the fixed-shaft type SFRS, including the RWA, MWA, etc. There have been many studies on the non-fixed-shaft type SFRS (mainly the CMG). From the point of view of concerns, they mainly focused on two aspects: (1) how to prevent the CMG falling into a dynamic singularity state [89–91]; (2) and how to reduce the spacecraft jitter caused by the disturbance of the CMG gimbal system [92–94]. However, from the perspective of structural dynamics, analytical modeling and analysis of micro-vibration disturbance characteristics of CMG are rare. Although the core component of the non-fixed-shaft type SFRS is still the high speed flywheel rotor, there is a significant inertial gyro coupling between the high speed rotor and gimbal rotor due to gimbal rotation. Based on the five degrees-of-freedom analytical model of the high speed rotor, Luo et al. [95] firstly established a micro-vibration analytical model of a single gimbal CMG (SGCMG), analyzed the combined stiffness characteristics, coupling dynamics, and disturbance output characteristics, and revealed the variation of apparent moment of inertia of the gimbal with high speed rotor speed. Based on the analytical model of SGCMG, they [96] also investigated the dynamic characteristics of a vibration isolation system with multiple SGCMGs. The results showed that the gyroscopic effect produced by the rotating flywheel leads to several structural modes of the coupling system, hard or soft. In addition, the gyroscopic effect of each SGCMG can interact with or counteract the gyroscopic effect of other SGCMGs, resulting in coupled vibration modes. On this basis, Shi et al. [97] adopted Luo's analytical mode for the analysis and design of an SGCMG vibration isolation platform. Li et al. [98] studied the micro-vibration characteristics of CMG combined with the dynamic test results, and analyzed the influence of a flexible interface on the micro-vibration characteristics of CMG using the dynamic substructure method [99]. Through modal test and frequency response analysis, Wu et al. [100] studied the transmission characteristics of micro vibration of CMG.

The micro vibration produced by the high-speed rotor of a CMG will affect the accuracy and stability of the CMG's output torque, reduce the stability of the CMG's low-speed gimbal control and the stability of the whole satellite attitude control, and directly affect the accuracy of vibration-sensitive equipment on board, such as reducing the imaging quality of a camera. Therefore, how to accurately predict the dynamic output torque of a CMG and realize the traceability of high frequency interference components is one of the key problems in high-performance spacecraft. In view of the leading role of the micro-vibration characteristics of a high speed rotor on the output torque, several scholars have studied the micro-vibration response of a high speed rotor from the perspective of dynamic analytical modeling, and then discussed its influence mechanism on the output torque. Zhang et al. [101] established a dynamic analytical model of a CMG, and analyzed the influence of static and dynamic imbalance and installation error of a high speed rotor on the high-frequency interference component of output torque. Furthermore, Zhang et al. [102] introduced the flexibility of the support isolation structure into the proposed analytical model, and conducted a dynamic analysis in the frequency domain for a CMG with an isolation system, which verified the effectiveness of the designed system. Based on the Newton-Euler method and moment of momentum theorem, considering the installation error of the flywheel and micro-vibration response of the flywheel rotor system, Wang and Han [103] derived the three-axis output torque of an SGCMG, characterized the coupling transmission mechanism between the micro vibration of a high-speed flywheel rotor and the output torque of the whole system, and discussed the effects of static and dynamic eccentricity of the flywheel, the amplitude of bearing surface waviness, bearing axial preload, and installation deflection angle on the output torque.

3.3. Hybrid Models

The hybrid model, also known as the semi-analytical model, regards the analytical model of the SFRS as a kind of specially designed filter, inputs the harmonic and broadband disturbances obtained from the empirical model, and finally obtains the output of the SFRS after calculation. Liu et al. [104] put forward the concept of the hybrid model for the first time:

$$\left[\begin{array}{l} f(t) = \sum_{i=1}^n C_i \Omega^2 \sin(2\pi h_i \Omega + \alpha_i) \\ Q_j(t) \end{array} \right] \xrightarrow[\text{Filtering}]{\text{Superposition}} [\text{hybrid models}] \rightarrow [M\ddot{x} + (G + C)\dot{x} + Kx = F(t)] \quad (3)$$

The hybrid model effectively combines the advantages of the empirical model and the analytical model. It can not only capture the structural dynamic characteristics of the SFRS, but also explain the wide-band disturbance of the SFRS at low speed. Liu et al. [104] applied it to interference modeling and jitter analysis of the RWA in SDO. Based on the hybrid model, Park et al. [105] defined the transmission mechanism of micro vibration of the RWA, and then successfully designed a multiple degrees-of-freedom micro-vibration simulator for spacecraft shaking test research. Aiming at the parameter identification problem involved in the hybrid model, Kim [106] proposed a two-step sequential optimization method, and verified the effectiveness of the proposed method through numerical and test results. Sanfedini et al. [107] applied the dual input–dual output method for hybrid modeling of the RWA, and combined it with the dynamic model of a space telescope with two flexible solar panels and antennas to investigate the possible coupling effect between the structural and RWA flexible modes. The analysis results have certain guiding significance for passive vibration isolation scheme design.

The focus of the hybrid model is to determine the specific amplitude of harmonic and broadband disturbance. In general, it should be determined by repeated calibration through tests. Several scholars have carried out fruitful work on the effective utilization of experimental data. Using the disturbance input matrix to quantify the response changes of different structures, Lellis et al. [108] developed a hybrid model. Practical application results showed that the model can describe the typical behavior of a series of micro-vibration sources of an RWA, and predict the worst case accurately with only a limited number of devices considered. Based on the measured data of disturbing forces and torques in a certain frequency band, Hur and Kim [109] proposed a hybrid model. The accuracy of the proposed model was verified by comparing the predicted results with the measured PSD function of the RWA. Through the additional evaluation method, the predicted response of a single cantilever beam was compared with the measured value during the actual operation of the RWA on the cantilever beam, which effectively improved the prediction ability of the hybrid model for operating vibration. On the basis of the established hybrid model, Hur [110] further proposed a source-path-receiver method for designing isolators of RWA to reduce angular vibration on a flexible satellite.

For the convenience of researchers, the review of micro-vibration models of the SFRS is summarized and listed in Table 1.

Table 1. Summary of micro-vibration models of the SFRS.

Model Types	Current Studies	SFRS Types	DoFs	Disturbances				Applications
				(A)	(B)	(C)	(D)	
Empirical	[53–58]	RWA	— —	√	√	x	x	Micro-vibration analysis of the whole spacecraft
	[59–62]	RWA	— —	√	√	x	√	Influence of assembly error on micro vibration
	[63,64]	CMG	— —	√	√	x	x	Multiple disturbances with higher accuracy in lower bandwidth

Table 1. Cont.

Model Types	Current Studies	SFRS Types	DoFs	Disturbances				Applications
				Ⓐ	Ⓑ	Ⓒ	Ⓓ	
Analytical	[19,65–67]	RWA	4	√	x	x	x	Natural characteristics and whirl response
	[68–76]	MWA	5 †	√	x	x	√	Dynamic coupling between the installation foundation and SFRS
	[77–80]	RWA	5 ‡	√	x	√	√	Torsional and radial vibrations of SFRS
	[81–84]	RWA	6	√	x	x	√	Dynamic coupling between SFRS and its bracket
	[85–88]	MWA	5 †	√	√	x	√	Nonlinear stiffness of rolling bearing and surface waviness excitation
	[95–103]	CMG	5 + 3 §	√	√	x	√	Micro-vibration and dynamic output torque characteristics of CMG
Hybrid	[104–107]	RWA	— —	√	x	x	x	Interference modeling and jitter analysis of the RWA in SDO
	[108–110]	RWA	— —	√	x	x	√	Typical behavior of a series of micro-vibration sources of RWA

Ⓐ: mechanical disturbance (rotor unbalance). Ⓑ: mechanical disturbance (bearing non-ideal characteristics). Ⓒ: electromagnetic disturbance. Ⓓ: structural disturbance. †: 4 DoFs + axial DoF. ‡: 4 DoFs + torsional DoF. §: 2 translational and 1 axial DoFs of the gimbal rotor.

4. Micro-Vibration Suppression of SFRSs

To date, two aspects of research have been examined to effectively reduce the micro vibration of SFRSs: (1) suppression of micro vibration source and (2) control of transmission path. Aspect (1) refers to the source suppression of SFRSs through structural innovation design, while aspect (2) designs various isolation devices to effectively reduce the transmission of micro vibration from the SFRS to the spacecraft. This section mainly reviews the progress on aspect (1), while the next section will focus on the recent developments in aspect (2).

4.1. Low Disturbance Flywheel Technology

In order to improve the moment of inertia and maintain a small mass, the flywheel usually has a complex spoke structure, which is realized by the assembly of multiple structural parts. The initial imbalance of the rotor is at a low level due to strict dynamic balancing. However, due to assembly error, working conditions change, material wear degradation, and other factors, the actual rotor imbalance still remains at a high level [111]. How to design a flywheel structure with low balance disturbance and suppression of micro vibration at the source is the goal pursued by many scholars. In the study of RWA for a nano-micro satellite, Inamori et al. [112] proposed use of a small size flywheel and limited flywheel speed to reduce balance disturbance. Obviously, this method will have many inconveniences when applied to medium and large spacecraft. Based on the principle of electromagnetic induction, Kim et al. [113] proposed a spherical reaction flywheel. Since it has no mechanical contact and can output control torque around any three axes in space, the influence of balance disturbance was greatly reduced. Nagbhusan and Fitz-Coy [114] proposed a novel multi-wheel structure, as shown in Figure 3. By controlling the rotation speed and phase of each wheel, the residual balance disturbance between various wheels can be cancelled or compensated, so as to reduce the overall disturbance output of the SFRS. This novel design does not require accurate dynamic balancing treatment of the flywheel, and has high reliability. When a single flywheel fails to work, other flywheels can work normally and achieve partial imbalance compensation to ensure low disturbance output. However, it is worth noting that this design introduces multiple groups of bearing systems, and the micro-vibration disturbance caused by the bearing system is generally nonlinear,

so it is difficult to eliminate the micro-vibration disturbance caused by the rolling bearing through the same method of controlling the rotation speed and phase.

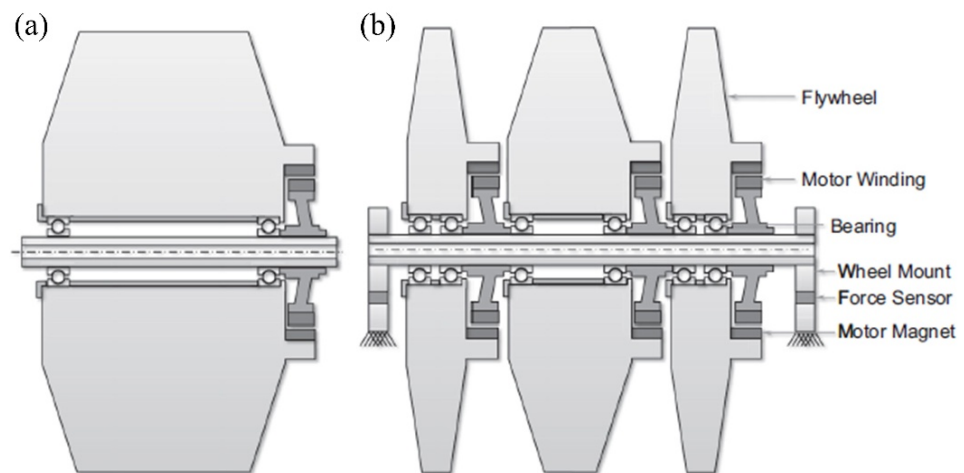


Figure 3. (a) Conventional SFRS with single wheel structure and (b) SFRS with a novel multi-wheel structure [114].

With the development of rotor dynamic balancing technology, much attention has been paid to automatic balancing technology in the process of operation. Automatic balancing is an automatic adjustment process in which the principle axis of rotor inertia coincides with its rotating axis by means of an automatic balancing device. According to whether the external energy is required or not, the automatic balancing devices include both passive and active types.

The passive type of automatic balancing device is mainly designed for a flexible rotor in supercritical state, including the ball type [115,116], balanced pendulum type [117,118], hydraulic type [119,120], etc. The passive type of automatic balancing device has the advantages of simple structure, high reliability, and no requirement of external energy. It has been successfully applied in washing machines and computer CD-ROM drives. However, its application in SFRSs is still limited due to the disadvantage of increasing rotor imbalance in the subcritical state. How to solve the problem of at least not increasing the initial rotor imbalance in the range below the first critical speed is the key problem in the design of passive automatic balancing devices.

In the active type of automatic balancing device, the balance head is installed on the rotor, and the size and orientation of the internal mass of the balance head are adjusted by the control system from the external input energy. The correction balance is generated to offset the original imbalance, and then achieve the purpose of balancing the rotor. The active type of automatic balancing device can be divided into electromagnetic [121,122], electromechanical [123], liquid spraying [124,125], etc. Electromagnetic or electromechanical balance heads generally contain two balance masses which can move along the circumference or in a radial direction. The relative position between them can be adjusted by electromagnetic or mechanical forces to obtain the correction balance. Liquid spraying balance heads include several fan-shaped cavities which are not connected with each other, and each of them corresponds to a nozzle. The flow rate of each nozzle can be effectively controlled to achieve rotor balance. The active type of automatic balancing device has the advantages of flexible adjustment, fast balancing speed, and high efficiency, and has a good balancing effect for both rigid and flexible rotors. At present, it is widely used in the design of motorized spindle rotors. However, active automatic balancing devices make great changes to the rotor structure and require an additional energy supply. For the SFRS, which has many limitations such as structure, mass and space, how to apply an active automatic balancing device still needs further research.

4.2. Elastic Supports

In addition to the design of flywheel structures with low balance disturbance, the supporting structure of the flywheel could be designed to have certain elastic and damping characteristics, which would also be beneficial to micro-vibration suppression for an SFRS. Aglietti et al. [68,69] put forward a flywheel technology based on elastic supports (see Figure 4), which are used to filter out the disturbance in the high frequency range by connecting the elastic support structure in series with the bearing inside the flywheel. Through a series of numerical simulations, the flywheel prototype was developed and verified to have good low disturbance characteristics by dynamic tests [70–73]. Satellite Service Ltd. manufactured a low-disturbance flywheel product based on this design, and has carried out aerospace application [68]. Kawak [126] proposed a novel two-stage viscoelastic structure to suppress shock vibration, structural resonance, and drive motor noise, respectively. The studied application on a small agile satellite showed that the attenuation provided by the two-stage viscoelastic support structure can reach a slope of -80 dB/dec. Huang et al. [127] proposed a flexible annular structure, which is supported on the wheel arms and inner edge through independent viscoelastic cushion blocks and elastic buffers, respectively. Both simulation and test results showed that the flexible structure can significantly suppress the radial and axial modal micro vibration of an SFRS at different speeds under the premise that the loss coefficient and proportional damping coefficient are greater than 0.2 and 6 Ns/m, respectively.

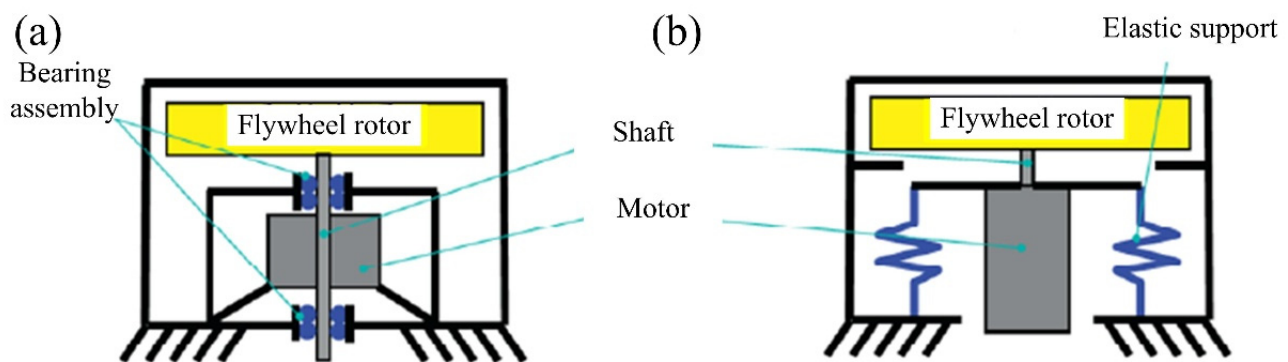


Figure 4. (a) Conventional SFRS with rigid supports and (b) SFRS with elastic supports [69].

Jacobs et al. [128,129] proposed an intelligent support structure based on the piezoelectric damping technique. The whole flywheel structure was not modified, and only an elastic gasket structure made of piezoelectric material was installed in the bearing assembly. The piezoelectric gasket can convert the micro-vibration energy into electrical energy for dissipation, and it can achieve wide band micro-vibration suppression by tuning the working frequency of the device. Hindle et al. [130] introduced an I-shaped flexure structure to adjust the radial length between the piezoelectric gasket and the bearing. The results showed that the flywheel structure is only slightly changed, and the impact of the quality of the additional piezoelectric gasket is usually small, which can be ignored. By improving the connection between the bearing system and housing, the technology is developing towards intelligent support of the rotor system, which is a good reference point for future SFRS design.

4.3. Maglev Bearing

At present, mechanical rolling bearings are widely used in SFRSs. By strictly controlling the machining and assembly accuracy (the accuracy level of most aerospace rolling bearings has reached P4), the non-ideal characteristics of bearing components, such as ovality, surface waviness, and friction characteristics, are at a low level. However, due to the inherent shortcomings of mechanical rolling bearings, such as contact friction, viscous torque, zero crossing dead zone, etc., significant mechanical disturbance is still produced

in real applications [131]. The introduction of new supporting technology to replace the traditional mechanical bearing is the direction of joint efforts of both academic and industrial circles.

Maglev bearings exhibit the advantages of no contact, no friction, no lubrication, high precision, and long service life. They allow the high speed rotor to rotate according to the inertial principle axis, thus effectively reducing the impact of imbalance on the performance of the actuator [132,133]. Through active vibration control, the vibration interference to the spacecraft can be greatly reduced. Therefore, an SFRS based on maglev bearings has been widely examined by researchers. The maglev RWA/MWA [134–136] and maglev CMG [137,138] have been designed successively.

There is still rotor balance disturbance, electromagnetic disturbance, and structural disturbance in SFRSs with maglev bearings. Using the magnetic bearing to control the micro vibration caused by these disturbances will produce control current, increase the power consumption of the system, and even lead to saturation of the power amplifier. How to suppress these disturbances has become the main problem to be solved in the application of maglev bearing in SFRSs [139]. To address the synchronous vibration of maglev SFRSs caused by balance disturbance, Liu et al. [140] proposed a vibration control method through the open-loop bearing force compensation and the adaptive notch filter. Both simulation and test results showed that the proposed method can effectively suppress the imbalance vibration of maglev SFRSs in the whole speed range. Tang et al. [141] extended this method with closed-loop control to suppress imbalanced vibration when the rotor speed of a maglev SFRS exceeds the critical speed. Based on multiple notch filters and adaptive synchronous compensation, Xu, Chen, and Zhang [142] proposed an automatic balancing method for a maglev SFRS. Considering the synchronous and frequency-varying characteristics of the imbalanced excitation of a maglev SFRS, Peng et al. [143] proposed a special micro-vibration suppression method based on the small gain theory, which can not only eliminate the synchronous current fluctuation, but also have a good compensation effect on the displacement stiffness fluctuation of the permanent magnet bias bearing. Based upon this, they [144] considered the control phase lag factor, and further proposed a high-precision synchronous micro-vibration suppression method.

The above research is mainly aimed at the maglev RWA or MWA. For a maglev CMG system, the angular motion of the gimbal would also impose additional load on the magnetic bearing, which increases the control difficulty. Aiming at the problem of fast uncertainty compensation for the maglev CMG, Basaran et al. [145] proposed a compound adaptive output feedback control strategy based on Lyapunov theory. Control simulations showed that the high speed rotor of the maglev CMG has stronger gyroscopic effect due to the non-contact support. Tang et al. [146] presented the concept of inertia ratio, to study the relationship between the rotor structure and gyroscopic effect. A cross-feedback control method with pre-modulation gain was proposed to effectively suppress the influence of gyroscopic effects in a wider speed range. The results can provide useful enlightenment for the mechanical design and gimbal stability research of maglev SFRSs.

Theoretically, the magnetic bearing can eliminate friction and suppress vibration, thus greatly improving the performance of SFRSs. However, due to the introduction of the control system, the bearing system becomes much more complex with high power consumption. As is well known, spacecraft have strict restrictions on the internal space and total mass of the system. How to use a maglev SFRS in aerospace engineering practice still needs to be solved [147].

For the convenience of researchers, the review of techniques for micro-vibration suppression of the SFRS is summarized and listed in Table 2.

Table 2. Summary of techniques for micro-vibration suppression of the SFRS.

Suppression Techniques	Current Studies	Advantages	Disadvantages	Applications
Low disturbance flywheel technology	Multi-wheel structure [114]	Low precision dynamic balancing treatment; high reliability	Difficult to eliminate disturbances of rolling bearing	Prototype
	Passive type of automatic balancing device [115–120]	Simple structure, high reliability, no requirement for external energy	Increasing imbalance in subcritical state	Not yet used in SFRSs
	Active type of automatic balancing device [121–125]	Flexible adjustment, fast balancing, balancing effect for both rigid and flexible rotors	Great changes to rotor structure, needs additional energy	Not yet used in SFRSs
Elastic supports	Viscoelastic damping material [68–73,126,127]	Passive type, high reliability, no requirement for external energy	Changes to the structure, limited effect on low-frequency micro vibration	Widely used in SFRSs
	Piezoelectric damping material [128–130]	Intelligent support, wide band micro-vibration suppression	Needs dissipative circuits	Prototype
Maglev bearing	[132–147]	No contact, no friction, no lubrication, high precision, long service life	Complex structure, high power consumption	Demonstration application in SFRSs

5. Micro-Vibration Isolation of SFRSs

In addition to the micro vibration suppression techniques, designing an isolation device is also an effective way to reduce the transmission of micro vibration from the SFRS to the platform. At present, a great number of isolation prototypes and products have been developed, including passive types, active types, and hybrid types [148]. According to the technical path, the existing micro-vibration isolation technologies can be divided into: (1) micro-vibration isolation based on a folded-beam structure; (2) micro-vibration isolation based on rod elements, and (3) micro-vibration isolation based on maglev technology. In addition, the introduction of nonlinear factors (including nonlinear damping and quasi-zero stiffness) to broaden the operational frequency band of a vibration isolation system, and improve its low-frequency vibration isolation performance, is also the direction of many scholars' efforts. The relevant progress will be reviewed in the following.

5.1. Micro-Vibration Isolation Based on a Folded Beam Structure

On the premise of not changing the internal structure of the SFRS, vibration isolation technology based on a folded-beam structure uses a low stiffness platform composed of multiple continuous short beams to reduce the installation stiffness between the SFRS and the spacecraft, and reduce the transmission of micro vibration between them. Kamesh et al. [149] first proposed the scheme (see Figure 5a), carried out the corresponding theoretical analysis and experimental research (see Figure 5b), and verified the effectiveness of the passive method for vibration isolation of RWA. Kamesh et al. [150] further pointed out that sticking piezoelectric intelligent material on the short beam can realize intelligent vibration isolation of an SFRS. However, the gyroscopic effect induced by the high speed rotor was ignored in the design of the folded-beam structure. In fact, the gyroscopic effect will change the frequency distribution of the rotor system, and thereby have an important impact on

the vibration characteristics of the system. Especially for a low stiffness gyroscopic system composed of a folded-beam structure and an SFRS, this effect might be significant.

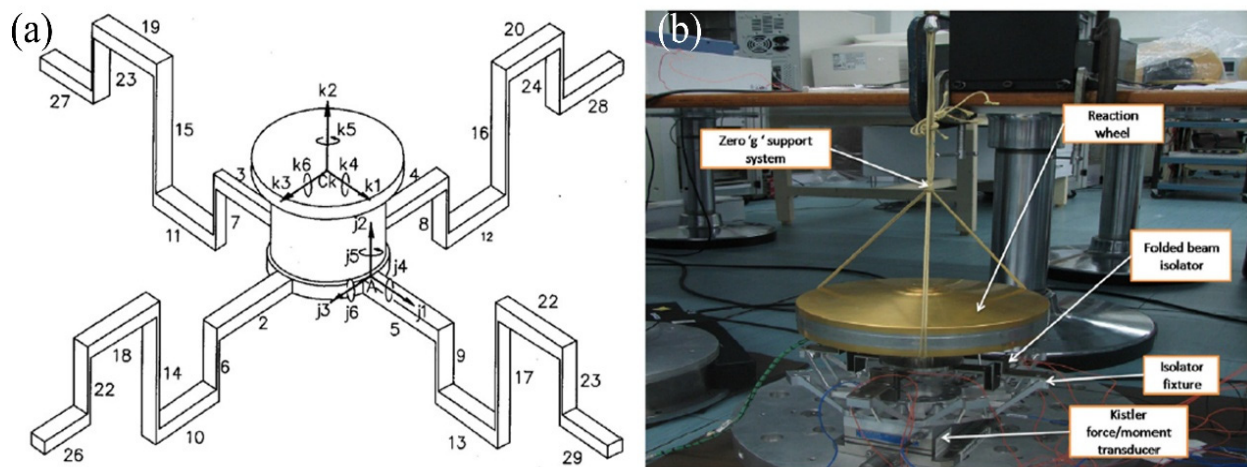


Figure 5. RWA with folded-beam structure isolator [149]: (a) schematic diagram and (b) dynamic test rig.

In view of this, Zhou et al. [151] proposed a similar folded-beam vibration isolation platform, and deduced an analytical model of RWA and vibration isolation device considering gyroscopic effects. Zhou et al. [152] further conducted a series of dynamic tests. On the basis of verification of the analytical model, it was pointed out that the flywheel rotation has a significant impact on the critical speed of the coupling system including the folded-beam structure, and should be paid full attention when designing the vibration isolation system. Wei et al. [153] conducted a study on the performance of the folded-beam vibration isolation device for an SFRS. The results demonstrated that the overall output disturbance of the SFRS can be minimized by optimizing the beam structure, but there is a compromise between the performances of the SFRS at different speeds. Using the finite element electromechanical coupling method, Luo et al. [154] analyzed the performance of the active folded-beam structure with a surface bonded piezoelectric actuator. A modal frequency shift method was proposed to widen the low frequency vibration isolation range. Numerical simulation results showed that the desired isolation effect can be achieved by using a hybrid response feedback method. By paralleling the spatial folded-beam structure with a negative-stiffness magnetic spring, Dong et al. [155] proposed a novel vibration isolator with “high-static low-dynamic” characteristics. The natural frequency of the isolator was reduced, and the low-frequency bandwidth was effectively widened. Through dynamic tests of the prototype, theoretical prediction results were verified.

Generally speaking, a vibration isolation platform based on the folded-beam structure has better passive (even active) isolation performance. However, it is usually suitable for fixed-axis type SFRS. For the non-fixed type SFRS, such a type of isolation platform might not be suitable.

5.2. Micro-Vibration Isolation Based on Rod Elements

A damping dissipation material is encapsulated into the cylindrical shell to realize the vibration isolation rod element. A vibration isolation rod unit for an SFRS requires long-term service in orbit, and its working environment is quite different from that of the traditional isolation rod unit on the ground. The vibration amplitude is usually in the order of micro-meters, and it also has to withstand severe conditions (radiation, vacuum, high and low temperatures alternating for a long time). After comparing the common damping dissipation forms of vibration isolation rod elements, as shown in Table 3, Zhang et al. [156] considered that the eddy current damper has certain advantages owing to its strong adaptability and high sensitivity. New metal damping materials, such as metal

rubber and steel wire rope, also have good application prospects. However, it is necessary to further verify their isolation performance under a micro-vibration environment in orbit. Based on the nonlinear dynamic modeling and fluid structure coupling analysis, Jiao et al. [157] considered that a viscous fluid damper can also be used for isolating the vibration of the SFRS.

Table 3. Comparison of several damping principles.

Damping Types	Advantages	Disadvantages	Applications
Viscous damping	Various forms, high damping ratio	Greatly affected by temperature, aging gassing problem, strength problem	Distributed, independent
Fluid damping	Large damping force	Potential leakage risk, easy to jam under zero gravity	Independent
Eddy current damping	All metal, high sensitivity	Relatively small damping force under the same volume	Used inside the vibration isolator
Dry friction damping	All metal	Sound effect only in large deformation	Used in joint parts
Particle damping	Not affected by temperature	Nonlinear, low energy-loss factor, only suitable for large load conditions, needs special design of anti-weight device	Independent cavity

Similar to vibration isolation platforms based on the folded-beam structure, the vibration isolation platform based on rod elements also does not change the internal structure of the SFRS, but uses several independent rod units with a certain topological configuration. There are many kinds of vibration isolation mechanisms, and the number and installation configuration of rod units can be designed arbitrarily under certain conditions. The vibration isolation method based on rod elements is more flexible and reliable, so it has been widely used in aerospace. At present, there are four kinds of vibration isolation platforms for SFRSs, including unidirectional platforms, three-leg platforms, six-leg platforms, and eight-leg platforms.

5.2.1. Unidirectional Platform

Only the axial isolation ability of the rod element is used in a unidirectional platform. The application of the unidirectional platform was first found in the axial vibration isolation of RWA in HST. Rodden et al. [158] installed the isolation rod unit parallel to the axial direction of the flywheel rotor to isolate the micro-vibration disturbance along the RWA axis. The rod element was made of a metal spring and viscous flow damper in parallel. The former can reduce axial support stiffness, while the latter can reduce the peak disturbance value. Wang and Zheng [159] proposed a transfer function method with two steps to improve the efficiency of parameter optimization design. Kown et al. [160] braided a superelastic shape-memory alloy wire into an annular structure for axial vibration isolation of RWAs. The experimental results showed that such an axial unit can effectively isolate the strong impact in the launch phase and the micro vibration in the orbit phase. When studying the influence of micro vibration of the SFRS on the imaging quality of space cameras, Li et al. [161] optimized the stiffness and damping characteristics of the axial vibration isolation rod element, and the image motion caused by the micro vibration was less than 0.1 pixel. Chen et al. [162] developed a dual axial vibration isolation unit, which can improve the attenuation rate (can reach 69.0%) in the high frequency band on the premise of keeping the structure compact.

All the above unidirectional platforms belong to the passive vibration isolation type, and thus have high reliability. However, the performance of this type of isolation platform is limited when dealing with the wide-band disturbance of the SFRS at variable speeds. Oh

et al. [163] adopted a metal spring and viscous flow damper to make a semi-active vibration isolation rod element. An actuator made of TiNi shape-memory alloy and a piston were used to adjust the damping characteristics of the viscous flow damper. Several rod elements were installed in the rotating plane to reduce the radial disturbance force. In the low-speed region, the throttle hole is closed to increase the viscous flow damping, while in the high-speed region, the throttle hold is opened to reduce the damping. Magliacano et al. [164] proposed an active vibration control (AVC) concept for vibration reduction. In the context of the presented activity, the floor panel was studied as a test case for an AVC implementation based on the use of piezoelectric actuators. A preliminary numerical activity was performed for the correct evaluation of the dynamic behavior of the system under specific external disturbance spectra. The principal results showed a good ability of the actuation system to manage the control signals in terms of vibrational energy; this outcome indicates that piezoelectric patches could be good candidates as adequate actuation devices.

Makihara et al. [165] designed three kinds of semi-active vibration isolation rod elements, which are composed of piezoelectric materials and switch-controlled passive circuits. Numerical simulations showed that the system can remain stable even if the control system fails. Zhang et al. [166] proposed a hybrid vibration isolation rod element composed of an active piezoelectric stack actuator and a passive rubber damper. Based on the establishment of dynamic models and the derivation of the transfer rate formula, a control algorithm was developed using the linear quadratic regulator method. Prototype tests showed that the hybrid isolator element can effectively eliminate the resonant peak, and the passive rubber damper can still isolate part of the vibration when the active controller fails. Wang et al. [167] also proposed a passive/active hybrid vibration isolator, by combining an oil-filled bellows (the passive element) and an inertial actuator (the active element). An adaptive control method based on the least mean square algorithm was adopted to suppress the transmission of micro vibrations caused by the sinusoidal, impulsive, and random disturbances. Dynamic tests showed that the passive rod element has a reasonable amplification factor, and the attenuation slope was -40 dB/dec. The inertial actuator can suppress both sinusoidal and random disturbances.

5.2.2. Three-Leg Platform

Generally speaking, the disturbance output of an SFRS is multi-directional, and the above-mentioned unidirectional vibration isolation is mainly aimed at one single direction (such as axial or radial). In order to improve generality, the rod units are usually assembled into a vibration isolation platform to realize multi-directional or even omni-directional isolation of the SFRS. According to the number of isolation rods, the multi-directional isolation platform is divided into three-leg platforms, six-leg platforms and eight-leg platforms. This section mainly describes research progress on three-leg platforms.

Guan et al. [168] made a multi-directional spring and metal rubber into a passive vibration isolation rod unit, and put forward a prototype of a three-leg platform. The introduction of a multi-directional spring can realize multi-directional vibration isolation of the SFRS, and compensate the additional displacement caused by the hinge clearance at both ends of the rod unit. However, it is difficult to ensure that each rod element has the same stiffness characteristics along various directions during manufacturing, which makes the support stiffness of the proposed three-leg platform uncertain.

If the degree of freedom of a single rod element can be limited, the above uncertainty can be reduced. In general, only expansion and contraction along the axial direction of the rod element are retained, therefore the three-leg platform has only three degrees of freedom. Zhao et al. [169] proposed a semi-active vibration isolation platform with three translational degrees of freedom. Based on a bellows and a viscous fluid damper, Lee et al. [170] designed a similar three-leg isolator. By improving the design of the bellows diaphragm and adopting a special heat treatment process, the isolator can withstand a large-amplitude vibration environment without permanent deformation during launching. In order to ensure good performance in orbit, the viscous fluid in the bellows was sealed under

vacuum conditions. The vibration isolation performance of the proposed three-leg isolation platform was systematically evaluated through ground simulation tests of launch impact and in-orbit micro vibration. A three-leg active vibration isolation platform is realized by Li et al. [171] by using the spatial parallel connection of three piezoelectric actuators and a proposed hybrid control strategy. Through dynamic testing of the prototype, the results demonstrated that the vibration isolation platform has a good low-frequency isolation performance (less than 10 Hz) along three translational directions.

In addition to translational degrees of freedom, the three-leg platform can also achieve rotational degrees of freedom. Based on the active piezoelectric actuator and the lever principle, the active three-leg isolation platform proposed by Kim et al. [172] can realize one translational and two rotational degrees of freedom in the mounting plane. Xu et al. [173,174] proposed a passive three-leg platform through a specially designed viscoelastic damping rod element, which achieved the same degree of freedom as Kim's platform [172]. Test results showed that the viscoelastic material has good energy-dissipation performance under micro-vibration conditions. Under sinusoidal excitation, white noise excitation, and given excitation, the acceleration response of the platform was significantly reduced, indicating that the proposed three-DoF three-leg platform can effectively suppress micro-vibration disturbance of the SFRS. To improve the low-frequency isolation performance of the platform, Xu et al. [175] further proposed an intelligent platform combined with a magnetic fluid damper, which has excellent isolation performance in a wide frequency range (0–500 Hz).

5.2.3. Six-Leg Platform

The three-leg platform cannot meet the requirement of omni-directional vibration isolation of the SFRS. The number of isolation rod units must be increased. As early as 1995, Spanos et al. [176] first proposed a six-leg vibration isolation platform for the MWA. The rod unit was made of a mechanical spring in parallel with the electromagnetic voice coil actuator. Force-feedback active control was applied to improve the passive vibration isolation performance. Six rod elements interacted with each other to realize omni-directional vibration isolation. Since the rod element has only one degree of freedom along the rod direction, the interaction between the rod elements in turn leads to motion coupling between the rod elements. Using the Stewart-Gough configuration, Spanos et al. [176] further designed the six rod elements as the six sides of a cube, arranging them in parallel or vertical relationships. The results demonstrated that the Stewart-Gough configuration can effectively reduce the coupling effect between various rod elements. Under small amplitude conditions, each rod element can be considered completely decoupled [177,178]. Pendergast et al. [179] designed a similar Stewart passive vibration isolation platform for each RMA on the Chandra telescope. Each isolation rod element was made of a mechanical spring and a viscoelastic material. The test results showed that the vibration isolation effect is obvious.

Lee et al. [180] proposed a hybrid vibration isolation platform based on the Stewart configuration for micro-vibration isolation of the RWA. The rod element was composed of two bellows springs and an electromagnetic voice coil actuator in series. Dynamic tests showed that the passive link can significantly suppress high-frequency disturbance, while the active link combined with a notch filter can significantly reduce low-frequency disturbance. Taking into account the difference of natural modes of each isolation rod of the Stewart platform, Yang et al. [181] proposed a dynamic isotropic design method, so that the non-zero natural frequencies of six rod elements were the same. Based on a decentralized active controller, the six-axis vibration control was decoupled into six identical controls of a single-axis vibration isolator. The uniform angular frequency and optimal active damping can be obtained by a Stewart-design platform. Furthermore, considering the additional stiffness caused by S-type and U-type flexible joints, Yang et al. [182] established a dynamic model of the six-axis vibration isolator of the flexible Stewart platform using a quasi-rigid model and virtual work principle, and then used that model for the decoupling controller

design. A Stewart six-leg vibrationisolation platform for MWAs of large space telescopes was designed by Qin et al. [183]. Based on the coupling dynamic model of telescope optical payloads and vibration isolation platforms, structural optimization was conducted to reduce the bandwidth of the integral mode of the telescope optical payload. Simulation and ground tests showed that the six-leg vibration isolation platform can significantly attenuate the disturbance transmitted to the optical payload of the telescope.

The Stewart configuration can effectively solve the coupling problem between the rod elements and provides convenience for active control. Therefore, in addition to the above six-leg platforms for SFRSs, researchers have also designed a great number of active Stewart platforms for vibration isolation of sensitive spacecraft loads and active control of precise pointing [184,185]. In general, these include two types: hard active mount (HAM) and soft active mount (SAM). The HAM usually uses actuators with a small stroke, such as piezoelectric ceramic actuators [186–189], magnetostrictive actuators [190], etc. For example, Anderson et al. [187] developed a satellite ultra-quiet isolation technology experiment. The actuator used in SAMs usually has a large stroke, such as voice coil linear motors [191,192] or permanent magnet/coil actuators [193,194]. For example, a six-leg isolation platform was developed by Thayer et al. [191]. Compared with the HAM, the SAM has a greater stroke, so it has a greater ability to accurately point and control sensitive loads. In addition, the lower support stiffness makes the vibration isolation frequency lower. However, in ground testing of the SAM, it is necessary to unload the gravity of a vibration-isolated load. It should also be fixed with bolts for launch protection, which may lead to inconsistencies between space and ground application and increase the uncertainty of the system.

Compared with isolation platforms based on the folded-beam structure, the advantage of Stewart-based six-leg vibration isolation platforms is that it is easy for them to achieve omni-directional isolation, and thus they can be applied to the vibration isolation of single or multiple SFRSs simultaneously. In fact, most of the CMGs on spacecraft are installed in clusters, and the groups of CMGs have pyramid, double-parallel, and other forms, which are chosen according to the requirements of specific space missions. The demand for diversity brings more space for application of the six-leg vibration isolation platform. Zhang et al. [195–199] conducted research on the isolation design of satellite CMG groups by using Stewart isolation-platform technology, and discussed the influence of isolation devices on flexible spacecraft accessories.

5.2.4. Eight-Leg Platform

Based on the six-leg platform, two isolation rod units are added to form the eight-leg platform, which improves the reliability of the system. The eight-leg isolation platform for CMGs group is designed by Heiberg et al. [200]. This special configuration integrated the vibration isolation platform and the CMG group, forming the idea of overall vibration isolation. The advantage of overall isolation is that it can greatly save volume and provide more valuable space for other payloads. The CMG groups of the World View-1 and -2 satellites launched by Digital Globe have adopted this integrated vibration isolation technology.

Recently, Huang et al. [201] reported a passive eight-leg isolation platform for a CMG group, and proposed an optimization method based on the frequency response function substructure method. Each isolation element consists of a metal rod and a three-parameter isolator in series. Numerical results showed that the proposed optimization method can be used in the design of an eight-leg platform. Luo et al. [202] used a constrained nonlinear multi-objective function to characterize the optimization problem of a passive eight-leg isolation platform, and proposed a hybrid genetic algorithm and sequential quadratic programming to obtain the optimal solution. Taking multiple MWAs with typical topology as an example, the optimization results and sensitivity of the theoretical model were verified.

5.3. Micro-Vibration Isolation Based on Maglev Technology

In addition to the above vibration isolation technology based on folded beam and rod elements, isolation technology based on maglev actuators has also attracted much attention in recent years. The research shows that maglev actuators have outstanding advantages, such as non-contact and long travel. Low-frequency vibration isolation could be realized through appropriate active control of the maglev actuator. To realize active control of a maglev vibration isolation platform, measuring the acceleration level with high precision is necessary. Wu et al. [203] developed a method to reduce the noise of angular acceleration measurement, and analyzed the influence of installation error and accelerometer azimuth error. Simulation and experimental results demonstrated that the method is suitable for a variety of maglev vibration isolation platforms. Gong et al. [204] conducted the system integration and control design of a 6-DoF maglev vibration isolation platform, and designed the necessary controller. In the range of 200 mrad, the attenuation ratio was 40 dB/dec in the low-frequency range (1–10 Hz). Conventional control methods mainly aim at specific payload tasks, and therefore lack versatility and transferability. Actual spacecraft payloads are often in dynamic unpredictable states. Self-decoupling and robust vibration control are necessary to realize the vibration control of maglev isolation platforms. Gong et al. [205] proposed a new control strategy, which was composed of a self-constructed radial basis function neural network inversion decoupling scheme (SRBFNNI) and a hybrid adaptive feed-forward internal model control (HAFIMC). The SRBFNNI enabled the maglev vibration isolation platform to establish the self-inverse model with less prior knowledge and realize self-decoupling. According to the particularity of maglev structures, a HAFIMC with adaptive parts dealing with periodic disturbance and internal model dealing with stability was proposed to solve the vibration control problem.

5.4. Micro-Vibration Isolation Using Nonlinear Factors

In recent years, many scholars have introduced nonlinear factors into vibration isolation systems based on nonlinear theory, which effectively widens the working frequency band of the vibration isolation system and improves low-frequency vibration isolation performance. To meet the ultra-high vibration isolation requirements of high-precision spacecraft, vibration isolation technology using nonlinear factors has good development potential. The nonlinear characteristic output spectrum (nCOS) was constructed to analyze and design vibration isolation systems with nonlinear factors. Jing et al. [148] reviewed the research progress in this field, and divided the nonlinear factors into two categories: nonlinear damping and nonlinear stiffness.

In terms of nonlinear damping vibration isolation technology, a viscoelastic damper with cubic nonlinearity is the most studied [206]. The traditional linear viscoelastic damping material has a narrow working frequency band. By introducing cubic nonlinearity, the working frequency band of the system has been greatly extended. Using the output frequency response function method, a cubic damping vibration isolation system with a single degree of freedom was analyzed and designed. The single degree-of-freedom system was extended to a multiple degrees-of-freedom system, and the influence of single or multiple cubic nonlinear damping effects on the system's transmissibility was studied. In addition, damping elements with geometric nonlinearity have also been successfully introduced into the isolation system [207]. The research progress of nonlinear viscoelastic-damping vibration isolation technology can be seen in Jing's review [148]. In addition to viscoelastic damping, the shunt-damping strategy, as an effective semi-active or passive control method, has attracted much attention owing to its low power consumption, lack of need for sensors, and high stability. Yan et al. [208–210] introduced the nonlinear factor into a traditional electromagnetic shunt-damping structure, and effectively widened the working bandwidth of the isolator by using the unique bistable characteristics of the nonlinear system. Stabile et al. [211] connected a negative resistance circuit with electromagnetic shunt damping to construct a semi-active damper, and proposed a design method. On this basis, they [212] extended it to a vibration isolation rod structure with two

collinear DoF, and manufactured a vibration isolation platform for the RWA. Theoretical and experimental results demonstrated that the two-stage damping provided by two separate electromagnetic shunt circuits can eliminate the resonance peak and obtain a significant attenuation rate of -80 dB/dec when applied to a suspension mass of 5 kg. The designed damping requirements and stability conditions can be achieved over a wide operating temperature range (-20 °C to $+50$ °C).

Although the dynamic response of natural frequencies or higher can be greatly attenuated by using nonlinear damping, the effect of vibration isolation is not ideal at a low-frequency band. Many scholars have explored the introduction of nonlinear stiffness to improve the performance of vibration isolation systems at a low-frequency band. Previous research progress shows that the vibration isolation system has high static stiffness and low dynamic stiffness (i.e., high-static low-dynamic, HSLD) through nonlinear stiffness design, such as quasi-zero stiffness and negative stiffness, so as to obtain ideal vibration isolation performance. Jing et al. [148] reviewed the research progress in this field. Recently, Zhou et al. [213] designed a vibration isolation rod with quasi-zero stiffness based on a specially designed cam roller spring mechanism, and arranged it in a pyramid shape to realize a quasi-zero stiffness vibration isolation platform with six degrees of freedom. To improve the vibration isolation performance of the passive Stewart platform, Zhang et al. [214] used a negative-stiffness magnetic spring to construct the HSLD strut. On the premise that the load capacity of the platform is not reduced, the resonant frequency can be effectively reduced. Then, they [215] connected the HSLD strut and a spatial swing mechanism in series to realize a passive multi-directional isolation platform. Palomares et al. [216] proposed a negative-stiffness system (NSS) based on two pneumatic linear actuators. Experimental results showed that the vibration attenuation rate was improved by 58% compared with a passive system without NSS. Jing et al. [217] first coupled the shear structure with a lever-type anti-resonant structure, and constructed a hybrid lever isolation system. The results showed that the hybrid system has good nonlinear characteristics, and can obtain a wider cut-off bandwidth by increasing the anti-resonant frequency. Recently, inspired by animal limb shapes in jumping and landing, Jing et al. [218,219] proposed a bionic vertical asymmetric X-shaped structure and systematically studied its vibration isolation performance. The results provided a new understanding of the modeling, gravity effect, asymmetry ratio and nonlinear response of X-shaped structures, which is helpful in the practical application of this kind of structure. Sun et al. [220] and Yang et al. [221] respectively introduced the parabolic cam roller negative-stiffness mechanism and three-bar linkage mechanism into the traditional shear structure, so that the constructed vibration isolation platform had an asymmetric and HLDS stiffness, which effectively improved the low-frequency isolation performance of the shear structure. In fact, in addition to using various means to achieve HLDS stiffness, the use of nonlinear energy sinks [222,223] and time delay effects [224] are also expected to improve the low-frequency vibration isolation performance of the platform.

For the convenience of researchers, the review of techniques for micro-vibration isolation of the SFRS is summarized and listed in Table 4.

Table 4. Summary of techniques for micro-vibration isolation of the SFRS.

Isolation Techniques	Current Studies	Advantages	Disadvantages	Applications
Folded beam structure	[149–155]	Simple structure; easy to achieve active isolation	Affected by gyroscopic effect; not suitable for non-fixed type SFRSs	Prototype
Rod element	Unidirectional platform [158–167]	Axial isolation; both semi-active/active isolation can be achieved; high reliability	Single direction isolation; unsuitable for multi-directional isolation	Widely used in SFRSs

Table 4. Cont.

Isolation Techniques	Current Studies	Advantages	Disadvantages	Applications
Rod element	Three-leg platform [168–175]	Multi-directional vibration isolation; both translational/rotational directions can be achieved; wider frequency range	Uncertainty exists in support stiffness; unsuitable for omni-directional isolation	Prototype
	Six-leg platform [176–199]	Omni-directional vibration isolation; both passive/active isolation can be achieved; good versatility	Motion coupling between rod elements; complicated structure	Used in actual SFRSs
	Eight-leg platform [200–202]	Omni-directional vibration isolation; suitable for groups of SFRSs; high reliability	Complicated structure; difficult to control	Used in actual SFRSs
Maglev technology	[203–205]	Non-contact; non-friction; long travel; suitable for low-frequency vibration isolation	Complicated structure; high power consumption	Prototype
Introduction of nonlinear factors	Nonlinear damping [206–212]	Wide operational frequency band; both semi-active/active isolation can be achieved	Poor performance in lower-frequency band	Prototype
	Nonlinear stiffness [213–221]	Excellent performance at low-frequency band; both passive/active isolation can be achieved; high static stiffness; low dynamic stiffness	Complicated structure; reliability needs to be improved	Prototype

6. Micro-Vibration Measurement Technology on the Ground

Ground testing is the most direct means to study the micro-vibration characteristics of an SFRS, and is also a necessary process to verify vibration isolation technology. The measurement method and system used in the experiment are the key to success. At present, the main measurement objects are disturbance force, structural acceleration, and displacement. Among them, the measurement method for disturbance force belongs to the direct method, and the latter two belong to the indirect method. Owing to the small amplitude, wide frequency band and strong randomness of the micro-vibration disturbance output of SFRSs, it is easy for them to be disturbed by external noise, such as mechanical vibration noise transmitted through the ground. In order to accurately capture the effective signal, the test system should be specially designed.

6.1. Disturbance Force Measurement

Based on the Kistler measurement table, Masterson et al. [54] established a set of systems which can directly measure the disturbance force and moment of an SFRS. During the test, the SFRS was fixed on the Kistler table, and the 12 force components can be measured through four internal force-sensing units. Then, six forces and six moments in the mounting surface can be obtained by the vector operation. The accuracy of the system was determined by the accuracy of the force sensor, which can reach up to 10.0 mN. Because of its direct measurement and piezoelectric force sensor, it can be classified as a rigid disturbance-force test platform. Based on this test platform, NASA has completed several types of SFRS disturbance tests. The performance of the vibration isolation device can be evaluated by comparing the disturbance output of the SFRS with and without the isolation device.

Kim [106], Kamesh et al. [149], and Chen et al. [225] also used Kistler tables to conduct disturbance tests of SFRSs and verification studies of vibration isolation devices. Considering the poor performance of piezoelectric force sensors in the low-frequency band, Chen

and Cheng [226] proposed a low-frequency compensation method, the effectiveness of which was verified by experiments. Then, it was applied to an SFRS disturbance-force test platform composed of eight single-axis piezoelectric force sensors. The prototype test showed that the proposed method can effectively compensate the low-frequency performance of the rigid test platform. Xia et al. [227] used eight piezoelectric force sensors to build a six-axis test platform for an SFRS. Theoretical analysis showed that redundant sensor placement can improve structural rigidity and test accuracy. The prototype test showed that the dynamic relative error is less than 5% and the static relative error is less than 5% in the range of 8–800 Hz. In the range of 40 kN, the linearity of the generalized force is in the range of 0.1% FS, while the repeatability is in the range of 0.1% FS.

To study the micro-vibration coupling between an SFRS and a flexible spacecraft platform, Elias [228] established a similar disturbance-test system using a JR3 force sensor. The JR3 sensor was installed between the flywheel and the flexible truss structure to measure the force and torque at the joint of the two components. The measurement accuracy of the system is mainly determined by the performance of the JR3 sensor. As the JR3 sensor was originally designed for an industrial robot, the accuracy is not high enough for micro-vibration measurement, but the method provides an important reference point for the study of coupling micro vibration between moving parts and a flexible spacecraft platform. Zhao et al. [229] built two test platforms to compare and analyze the disturbance output characteristics of RWA under rigid and flexible support boundary conditions. The measuring principle of the rigid test platform was similar to that of the Kistler table. The disturbing force and moment on the mounting surface were measured by six high-precision force sensors, as shown in the figure. The flexible test platform was composed of steel cables, static/dynamic force sensors, and a rigid installation adapter. The steel cables were used to simulate the flexible boundary, the static force sensor was used to ensure the consistency of the flexible cable boundary, and the dynamic force sensor was used to measure the disturbance signal of the RWA during operation.

6.2. Structural Acceleration Measurement

Aglietti et al. [68–70] designed a set of indirect micro-vibration measurement systems based on the acceleration signal of a seismic mass block, as shown in Figure 6. In comparison with direct measurement using a Kistler table, the correctness of the method was verified. The system consists of three parts: seismic mass block, acceleration sensor, and flexible support. An elastic rope was used to suspend the mass and RWA group to simulate free-free boundary conditions. Additionally, the interference of mechanical vibration noise transmitted from the ground was avoided. Four acceleration sensors were installed on the seismic mass block, as shown in Figure 6. The disturbance force and moment of the RWA were calculated by using the measured acceleration signal, the mass and inertia characteristics of the system, and the sensor position. The system is simple, effective, and low cost. Theoretically, the measurement accuracy can reach the order of 1.0 mN. However, the accuracy of the system was reduced in the process of converting acceleration into disturbing force and moment, because the position of the mass center cannot be accurately established.

6.3. Structural Displacement Measurement

Taniwaki et al. [230] developed a set of air-floating laser disturbance measurement systems based on displacement response, and completed the vibration isolation design verification of a flywheel mechanism by using this system. The flywheel is installed on the air-floating sliding block. The bottom and two sides of the slider are supported by air suspension, and only translational degrees of freedom in the X-dimension are obtained. The displacement of the slider can be measured by the laser sensor, and the interference force can be calculated by the displacement curve combined with the mass characteristics of the flywheel and the plate. The accuracy of the measurement system is very high, and the resolution of the radial disturbance force of the flywheel is about 1.0 mm under the steady

state. The measurement accuracy of the system is mainly affected by the Coulomb friction between the slider and the air cushion, and the stability of the air pressure and air flow in the air flotation system. Taniwaki et al. [231] increased the number of laser displacement sensors to 4 and successfully realized the high-precision measurement of low-frequency and low-amplitude disturbance torque.

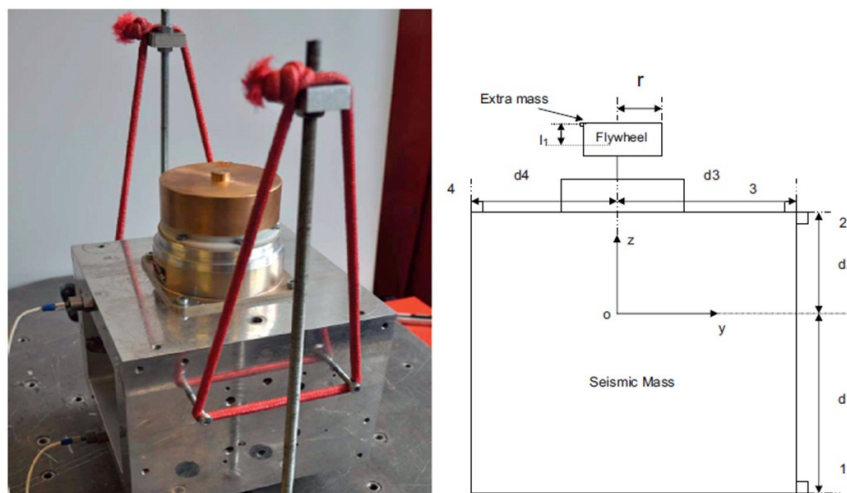


Figure 6. Micro-vibration measurement system based on the acceleration signal of a seismic mass block [69].

6.4. Micro-Vibration Simulator

In addition to building experimental platforms to test micro-vibration disturbance, some scholars also discussed micro-vibration simulators. Xu et al. [232,233] designed a six degrees-of-freedom simulator based on the structure of a six-bar Stewart vibration isolation platform, which is used to reproduce the interference force and torque generated by the RWA. Based on the study of the dynamic relationship between the acting force and disturbing force, and torque of tuning fork coil motor, a closed-loop iterative control method was developed, and the effectiveness of the control strategy was verified by comprehensive simulations. The disturbance force and torque reproduced by the simulator were tested on a six-component test bench. The results demonstrated that the maximum relative error between the measured value and the target value was 3.33%. The simulator can reproduce the disturbance force and torque produced by the SFRS, and has great application potential in ground-based micro-vibration experiments.

7. Existing Problems and Future Research Directions

7.1. Micro-Vibration Models of SFRSs

Existing models can accurately predict the main micro-vibration frequencies (including speed of rotation, power frequency and its doubling, bearing frequency, and rotor whirl frequency), and the relative error can be controlled within 5%. However, there is a great error between the amplitude prediction results and the measured results, and the relative error can reach 50% or even higher. This is because existing models can not accurately consider the influence of the actual residual imbalance of the rotor, the surface waviness of the rolling bearing, the structural machining error, the assembly clearance, and other nonlinear factors. Based on load identification, model updating, and measurement techniques, a fine and high-fidelity analysis model of SFRSs should be established to accurately predict the amplitude of micro-vibration response, after which sensitivity analysis and transmission characteristics research should be conducted, providing a theoretical basis for the design and monitoring of SFRSs.

Existing models are proposed for fixed-shaft SFRSs (including RWA and MWA). For non-fixed-shaft SFRSs (such as CMG), there are few modeling and analysis methods to

study their micro-vibration characteristics. Although the core component of the CMG is still a high-speed flywheel rotor, there is inertial gyro coupling between the high-speed rotor and the gimbal rotor due to the rotation of the gimbal. This coupling effect has a significant impact on the micro-vibration characteristics of SFRSs with non-fixed shaft. Based on the theory of structural dynamics, a micro-vibration analysis model of CMGs should be established to accurately characterize the inertial gyro coupling effect caused by gimbal rotation, analyze the micro-vibration mechanism and transmission mechanism of non-fixed-shaft SFRSs, and clarify the transmission characteristics of system dynamic output torque and the source of interference factors.

7.2. Micro-Vibration Suppression of SFRSs

In terms of low disturbance flywheel technology, active automatic balancing technology has good prospects for application. However, active automatic balancing devices require major changes to the rotor structure and additional energy supply devices. For an SFRS which has many limitations in structure, mass, and space, how to apply the active automatic balancing technology still requires further research.

Piezoelectric gasket-type elastic support structures have the advantages of small added mass, fast response, and low energy consumption. By improving the technology of connecting the bearing system with the housing, the SFRS can be made intelligent. Long-life and high-reliability piezoelectric ceramic materials suitable for the extreme environments of aerospace applications should be developed, and the optimal position configuration and control algorithm of sensitive elements and actuating elements in vibration control systems based on piezoelectric intelligent materials should be studied.

Theoretically, magnetic bearings can eliminate friction and restrain vibration, so as to greatly improve the performance of the SFRS. On the premise of not increasing the system mass and power consumption, an efficient control method suitable for magnetic bearings is proposed to effectively suppress the micro vibration caused by flywheel rotor balance disturbance, electromagnetic disturbance, and structural disturbance, and further improve the self-stability and anti-interference ability of magnetic bearings, which is a direction for future study.

7.3. Micro-Vibration Isolation of SFRSs

Vibration isolation platforms based on a folding-beam structure have better passive vibration isolation performance and excellent active control ability after extended design. They are generally only suitable for a single fixed-shaft type SFRS. On the premise of not changing the internal structure of the SFRS system, a new spatial topology of folding beams should be proposed, combined with advanced active control technology to effectively isolate the CMG from micro vibration.

The micro-vibration output of the SFRS is multi-directional. To improve universality, the vibration isolation rod unit is generally assembled into a vibration isolation platform to realize multi-directional or even omni-directional vibration isolation of the SFRS. However, increasing the number of vibration isolation rods will increase the mass and complexity of the system. In practical application, the mutual coupling between multiple vibration isolation rods will affect the overall vibration isolation performance. A new topological configuration of vibration isolation platforms should be proposed to improve the omni-directional vibration isolation performance. New damping dissipative materials should be introduced to meet the ultra-high requirements of extreme aerospace environments (radiation, vacuum, alternating high and low temperatures, etc.) for long-term stable service.

Nonlinear damping and stiffness have been introduced to effectively broaden the frequency bandwidth of the vibration isolation system and improve low-frequency vibration isolation performance. The stability and bifurcation of main resonance, subharmonic resonance, and superharmonic resonance of nonlinear vibration isolation systems should be studied, and the design level of nonlinear vibration isolation systems should be improved

from the perspective of stability margin and attraction region, so as to meet the ultra-high vibration isolation requirements at micro-meter amplitudes of the SFRS.

7.4. Micro-Vibration Measurement Technology on the Ground

Because the micro-vibration disturbance output of the SFRS generally has the characteristics of small amplitude, wide frequency band, and strong randomness, it is easy for it to be disturbed by external noise, such as mechanical vibration noise transmitted from the ground. To accurately acquire effective signals, the test system must be specially designed. In addition to the test technologies mentioned in this paper, a vibration isolator with high static stiffness and low dynamic stiffness can be introduced, which can effectively simulate the free state in orbit and isolate the low-frequency vibration interference from the ground under the condition of compensating for the effect of gravity on the SFRS.

8. Conclusions and Prospects

The main excitation sources of micro vibration of SFRSs are briefly described, and then the research progress is systematically reviewed from four perspectives, including the modeling methods, suppression means, vibration isolation techniques, and ground simulation tests. Finally, the existing problems of current research and the direction of further research are given to better serve the micro-vibration prediction and sensitivity analysis of the existing models, and provide reference points for micro-vibration suppression and isolation in the next generation of high-precision spacecraft.

Author Contributions: Conceptualization, Q.H. and S.G.; investigation, Q.H.; resources, S.G.; writing—original draft preparation, Q.H.; writing—review and editing, S.G.; supervision, F.C.; project administration, Q.H.; funding acquisition, Q.H. All authors have read and agreed to the published version of the manuscript.

Funding: This research was funded by National Natural Science Foundation of China grant number 12272199, and the State Key Laboratory of Tribology grant number SKLT2021D11.

Data Availability Statement: The data that support the findings of this study are available from the corresponding author upon reasonable request.

Acknowledgments: The authors would like to express the gratitude to the master student (Tenghao Ma) who assisted the authors in revising the format of the manuscript.

Conflicts of Interest: The authors declare no conflicts of interest.

References

1. Zhang, Y.; Jiang, J.; Zhang, G.; Lu, Y. High-accuracy location algorithm of planetary centers for spacecraft autonomous optical navigation. *Acta Astronaut.* **2019**, *161*, 542–551. [[CrossRef](#)]
2. Akhmetov, R.; Ereemeev, V.; Kuznecov, A.; Myatov, G.; Poshekhnov, V.; Stratilatov, N. High-precision geolocation of earth surface images from the resurs-p spacecraft. *Izv. Atmos. Ocean. Phys.* **2017**, *53*, 1155–1163. [[CrossRef](#)]
3. Pong, C. *High-Precision Pointing and Attitude Estimation and Control Algorithms for Hardware-Constrained Spacecraft*; Massachusetts Institute of Technology: Cambridge, MA, USA, 2014.
4. Lee, D.; Vukovich, G.; Lee, R. Robust adaptive unscented Kalman filter for spacecraft attitude estimation using quaternion measurements. *J. Aerosp. Eng.* **2017**, *30*, 04017009. [[CrossRef](#)]
5. Liu, C.; Ye, D.; Shi, K.; Sun, Z. Robust high-precision attitude control for flexible spacecraft with improved mixed control strategy under poles assignment constraint. *Acta Astronaut.* **2017**, *136*, 166–175. [[CrossRef](#)]
6. Marshall, T.; Gunderman, T.; Mobley, F. Reaction wheel control of the MSX satellite. In Proceedings of the Annual Rocky Mountain Guidance and Control Conference, San Diego, CA, USA, 2–6 February 1991.
7. Zhang, R. *Satellite Orbit Attitude Dynamics and Control*; Beijing University of Aeronautics and Astronautics Press: Beijing, China, 1998. (In Chinese)
8. Miller, D.; Weck, O.; Uebelhart, S.; Grogan, R.; Basdogan, I. Integrated dynamics and controls modeling for the space interferometry mission. In Proceedings of the IEEE Aerospace Conference Proceedings, Big Sky, MT, USA, 10–17 March 2001.
9. Miller, S.E.; Kirchman, P.; Sudey, J. Reaction wheel operational impacts on the goes jitter environment. In Proceedings of the AIAA Guidance, Navigation and Control Conference and Exhibit, Hilton Head, SC, USA, 20–23 August 2007.

10. Kim, Y.K.; Koo, J.H.; Kim, K.S. Vibration isolation strategies using magneto-rheological elastomer for a miniature cryogenic cooler in space application. In Proceedings of the IEEE/ASME International Conference on Advanced Intelligent Mechatronics, Montreal, QC, Canada, 6–9 July 2010; pp. 1203–1206.
11. Pong, C.M.; Smith, M.W.; Knutson, M.W. One-arcsecond line-of-sight pointing control on exoplanetsat, a three-unit cubesat. *Adv. Astronaut. Sci.* **2011**, *141*, 11–35.
12. Iyer, A.; Singh, S.N. Non-linear momentum and attitude control of a space station accommodating periodic aerodynamic disturbance. *Acta Astronaut.* **1995**, *35*, 391–402. [[CrossRef](#)]
13. Qu, Y.; Lu, C.; Li, T.; Yin, H. Research status and development prospect of high resolution satellite micro vibration. *Aerosp. China* **2014**, *8*, 22–24. (In Chinese)
14. Davis, L.; Wilson, J.; Jewell, R. *Hubble Space Telescope Reaction Wheel Assembly Vibration Isolation System*; NASA Marshall Space Flight Center: Huntsville, AL, USA, 1986.
15. Hyde, T.; Davis, L. *Vibration Reduction for Commercial Optical Inter-Satellite Communication Links*; SPIE Conference on Smart Structures and Integrated Systems: San Diego, CA, USA, 1998; pp. 94–105.
16. Lee, A.; Yu, J.; Kahn, P. Space interferometry mission spacecraft pointing error budgets. *IEEE Trans. Aerosp. Electron. Syst.* **2002**, *38*, 502–514. [[CrossRef](#)]
17. Watkins, R.; Agrawal, B.; Shin, Y.; Chen, H. Jitter control of space and airborne laser beams. In Proceedings of the 22nd AIAA International Communications Satellite Systems Conference & Exhibit, Monterey, CA, USA, 9–12 May 2004.
18. Masterson, R.A.; Miller, D.W. Development and validation of empirical and analytical reaction wheel disturbance models. In Proceedings of the AIAA/ASME/ASCE/AHS/ASC Structures, Structural Dynamics and Materials Conference, St. Louis, MO, USA, 12–15 April 1999; pp. 1–10.
19. Bialke, B. High fidelity mathematical modeling of reaction wheel performance. *Adv. Astronaut. Sci.* **1998**, *98*, 483–496.
20. Yang, X.; Chang, L.; Jin, G. Influence of dynamic imbalance of SGCMG rotor on remote sensing satellite imaging. *Chin. Opt.* **2012**, *5*, 358–365.
21. Genta, G. *Dynamics of Rotating Systems*; Springer Science+Business Media, Inc.: New York, NY, USA, 2004.
22. Wensing, J.A. *On the Dynamics of Ball Bearings*; University of Twente: Enschede, The Netherlands, 1998.
23. Tallian, T.E.; Gustafsson, O.G. Progress in rolling bearing vibration research and control. *Trans. ASLE Tribol. Trans.* **1965**, *8*, 195–207. [[CrossRef](#)]
24. Jang, G.H.; Jeong, S.W. Nonlinear excitation model of ball bearing waviness in a rigid rotor supported by two or more ball bearings considering five degrees of freedom. *Trans. ASME J. Tribol.* **2002**, *124*, 82–90. [[CrossRef](#)]
25. Jang, G.H.; Jeong, S.W. Vibration analysis of a rotating system due to the effect of ball bearing waviness. *J. Sound Vib.* **2004**, *269*, 709–726. [[CrossRef](#)]
26. Bai, C.Q.; Xu, Q.Y. Dynamic model of ball bearings with internal clearance and waviness. *J. Sound Vib.* **2006**, *294*, 23–48.
27. Babu, C.K.; Tandon, N.; Pandey, R.K. Vibration modelling of a rigid rotor supported on the lubricated angular contact ball bearings considering six degrees of freedom and waviness on balls and races. *Trans. ASME J. Vib. Acoust.* **2012**, *134*, 1–12. [[CrossRef](#)]
28. Wang, L.Q.; Cui, L.; Zheng, D.Z. Nonlinear dynamics behaviors of a rotor roller bearing system with radial clearances and waviness considered. *Chin. J. Aeronaut.* **2007**, *21*, 86–96.
29. Cao, M.; Xiao, J. A comprehensive dynamic model of double-row spherical roller bearing: Model development and case studies on surface defects, preloads, and radial clearance. *Mech. Syst. Signal Process.* **2008**, *22*, 467–489. [[CrossRef](#)]
30. Zhang, X.; Han, Q.; Peng, Z.; Chu, F. A new nonlinear dynamic model of the rotor-bearing system considering preload and varying contact angle of the bearing. *Commun. Nonlinear Sci. Numer. Simul.* **2015**, *22*, 821–841. [[CrossRef](#)]
31. Han, Q.; Chu, F. Nonlinear dynamic model for skidding behavior of angular contact ball bearings. *J. Sound Vib.* **2015**, *354*, 219–235. [[CrossRef](#)]
32. Randall, R.; Antoni, J.; Clapp, B. Rolling element bearing diagnostics: A tutorial. *Mech. Syst. Signal Process.* **2011**, *25*, 485–520. [[CrossRef](#)]
33. Jin, L.; Xu, S. Dynamic modeling and low rate control of gimbal servo system for single gimbal control moment gyro. *Chin. Space Sci. Technol.* **2010**, *12*, 1–10.
34. Muszynska, A. Rotor to stationary element rub-related vibration phenomena in rotating machinery-literature survey. *Shock Vib. Dig.* **1989**, *21*, 3–11. [[CrossRef](#)]
35. Chu, F.; Lu, W. Experimental observation of nonlinear vibrations in a rub-impact rotor system. *J. Sound Vib.* **2005**, *283*, 621–643. [[CrossRef](#)]
36. Chu, F.; Lu, W. Stiffening effect of the rotor during the rotor-to-stator rub in a rotating machine. *J. Sound Vib.* **2007**, *308*, 758–766. [[CrossRef](#)]
37. Pennachi, P.; Bachschmid, N.; Tanzi, E. Light and short arc rubs in rotating machines: Experimental tests and modeling. *Mech. Syst. Signal Process.* **2009**, *23*, 2205–2227. [[CrossRef](#)]
38. Jacquet-Richardet, G.; Torkhani, M.; Cartraud, P. Rotor to stator contacts in turbomachines: Review and application. *Mech. Syst. Signal Process.* **2013**, *40*, 401–420. [[CrossRef](#)]
39. Ma, H.; Yin, F.L.; Guo, Y.Z. A review on dynamic characteristics of blade-casing rubbing. *Nonlinear Dyn.* **2016**, *84*, 437–472. [[CrossRef](#)]

40. Wie, B.; Bailey, D.; Heiberg, C. Singularity robust steering logic for redundant single-gimbal control moment gyros. *J. Guid. Control Dyn.* **2001**, *24*, 865–872. [[CrossRef](#)]
41. Gustavsson, R.; Aidanpaa, J. The influence of nonlinear magnetic pull on hydropower generator rotors. *J. Sound Vib.* **2006**, *297*, 551–562. [[CrossRef](#)]
42. Lundstrom, N.; Aidanpaa, J. Dynamic consequences of electromagnetic pull due to derivations in generator shape. *J. Sound Vib.* **2007**, *301*, 207–225. [[CrossRef](#)]
43. Akiyama, Y. Unbalanced heating phenomenon of induction motor with eccentric rotor. In Proceedings of the IEEE Industry Applications Society Annual Meeting, Huston, TX, USA, 4–9 October 1992; pp. 107–114.
44. Dorrell, D. Sources and characteristics of unbalanced magnetic pull in three-phase cage induction motors with axial-varying rotor eccentricity. *IEEE Trans. Ind. Appl.* **2011**, *47*, 12–24. [[CrossRef](#)]
45. Zhu, Z.Q.; Mohd-Jamil, M.; Wu, L. Influence of slot and pole number combinations on unbalanced magnetic force in PM machines with diametrically asymmetric windings. *IEEE Trans. Ind. Appl.* **2013**, *49*, 19–30. [[CrossRef](#)]
46. Xu, X.; Han, Q.; Chu, F. A four degrees-of-freedom model for a misaligned electrical rotor. *J. Sound Vib.* **2015**, *358*, 356–374. [[CrossRef](#)]
47. Xu, X.; Han, Q.; Chu, F. Nonlinear vibration of a generator rotor with unbalanced magnetic pull considering both dynamic and static eccentricities. *Arch. Appl. Mech.* **2016**, *86*, 1521–1536. [[CrossRef](#)]
48. Xu, X.; Han, Q.; Chu, F. A general electromagnetic excitation model for electrical machines considering the magnetic saturation and rub impact. *J. Sound Vib.* **2018**, *416*, 154–171. [[CrossRef](#)]
49. Friswell, M.; Penny, J.; Garvey, S.; Lees, A. *Dynamics of Rotating Machines*; Cambridge University Press: New York, NY, USA, 2010.
50. Harris, T.A.; Kotzalas, M.N. *Rolling Bearing Analysis*; Taylor & Francis: Boca Raton, FL, USA, 2007.
51. Zhang, X.; Han, Q.; Peng, Z.; Chu, F. Stability analysis of a rotor-bearing system with time-varying bearing stiffness due to finite number of balls and unbalanced force. *J. Sound Vib.* **2013**, *332*, 6768–6784. [[CrossRef](#)]
52. Zhang, X.; Han, Q.; Peng, Z.; Chu, F. A comprehensive dynamic model to investigate the stability problems of the rotor-bearing system due to multiple excitations. *Mech. Syst. Signal Process.* **2016**, *70*, 1171–1192. [[CrossRef](#)]
53. Harsha, M. Reaction Wheel Mechanical Noise Variations. *Space Telesc. Program Eng. Memo SSS* **1986**, *218*, 175–183.
54. Masterson, R.; Miller, D.; Grogan, R. Development and validation of reaction wheel disturbance models: Empirical model. *J. Sound Vib.* **2002**, *249*, 575–598. [[CrossRef](#)]
55. Zhao, Y.; Sun, J.; Tian, H. Development of methods identifying parameters in reaction wheel assembly disturbance model. *Aircr. Eng. Aerosp. Technol.* **2006**, *78*, 326–330. [[CrossRef](#)]
56. Bai, Z.; Zhao, Y.; Ma, W.; Wang, Y. Effects analysis of reaction wheel disturbance on structure dynamics characters of spacecraft. *J. Astronaut.* **2009**, *30*, 2073–2079.
57. Yin, X.; Xu, Y.; Sheng, X.; Shen, Y. Signal denoising method using AIC-SVD and its application to micro-vibration in reaction wheels. *Sensors* **2019**, *19*, 5032. [[CrossRef](#)]
58. Shields, J.; Pong, C.; Lo, K.; Jones, L.; Mohan, S.; Marom, C.; McKinley, I.; Wilson, W.; Andrade, L. Characterization of cubesat reaction wheel assemblies. *J. Small Satell.* **2017**, *6*, 565–580.
59. Elias, L.; Miller, D. A coupled disturbances analysis method using dynamic mass measurement techniques. In Proceedings of the AIAA/ASME/ASCE/AHS/ASC Structures, Structural Dynamics, and Materials Conference, Denver, CO, USA, 22–25 April 2002; p. 1252.
60. Elias, L.; Dekens, F.; Basdogan, I.; Sievers, L.; Neville, T. A methodology for modeling the mechanical interaction between a reaction wheel and a flexible structure. In Proceedings of the SPIE 4852, Interferometry in Space, Waikoloa, HI, USA, 26 February 2003.
61. Shigemune, T.; Yoshiaki, O. Experimental and numerical analysis of reaction wheel disturbances. *JSME Int. J.* **2003**, *46*, 519–526.
62. Xia, M.; Qin, C.; Wang, X.; Xu, Z. Modeling and experimental study of dynamic characteristics of the moment wheel assembly based on structural coupling. *Mech. Syst. Signal Process.* **2021**, *146*, 107007. [[CrossRef](#)]
63. Huang, L.; Wu, Z.; Wang, K. High-precision anti-disturbance gimbal servo control for control moment gyroscopes via an extended harmonic disturbance observer. *IEEE Access* **2018**, *6*, 66336–66349. [[CrossRef](#)]
64. Huang, L.; Wu, Z.; Wang, K. Indirect measurement of rotor dynamic imbalance for control moment gyroscopes via gimbal disturbance observer. *Sensors* **2018**, *18*, 1873. [[CrossRef](#)] [[PubMed](#)]
65. Masterson, R. *Development and Validation of Empirical and Analytical Reaction Wheel Disturbance Models*; Massachusetts Institute of Technology: Cambridge, MA, USA, 1999.
66. Li, L.; Dai, J. Inner disturbance modeling and simulation analysis of reaction wheel system. *J. Syst. Simul.* **2005**, *17*, 1855–1859.
67. Deng, R.; Hu, G.; Wang, Q. Whirling characteristics of high speed rotors in flywheel and CMG. *Aerosp. Control Appl.* **2009**, *35*, 56–60.
68. Zhang, Z.; Aglietti, G.; Zhou, W. Microvibrations induced by a cantilevered wheel assembly with a soft-suspension system. *AIAA J.* **2011**, *49*, 1067–1079. [[CrossRef](#)]
69. Zhou, W.; Aglietti, G.; Zhang, Z. Modelling and testing of a soft suspension design for a reaction/momentum wheel assembly. *J. Sound Vib.* **2011**, *330*, 4596–4610. [[CrossRef](#)]
70. Zhang, Z.; Aglietti, G.; Ren, W. Microvibration model development and validation of a cantilevered reaction wheel assembly. *Appl. Mech. Mater.* **2012**, *226–228*, 133–137. [[CrossRef](#)]

71. Zhang, Z.; Aglietti, G.; Ren, W. Coupled microvibration analysis of a reaction wheel assembly including gyroscopic effects in its accelerance. *J. Sound Vib.* **2013**, *332*, 5748–5765. [[CrossRef](#)]
72. Addari, D.; Aglietti, G.; Remedia, M. Experimental and numerical investigation of coupled microvibration dynamics for satellite reaction wheels. *J. Sound Vib.* **2017**, *386*, 225–241. [[CrossRef](#)]
73. Addari, D.; Aglietti, G.; Remedia, M. Dynamic mass of a reaction wheel including gyroscopic effects: An experimental approach. *AIAA J.* **2017**, *55*, 274–285. [[CrossRef](#)]
74. Peng, C.; Fang, J.; Cui, P. Dynamics modeling and measurement of the microvibrations for a magnetically suspended flywheel. *IEEE Trans. Instrum. Meas.* **2015**, *64*, 3239–3252. [[CrossRef](#)]
75. Luo, Q.; Li, D.; Zhou, W. Studies on vibration isolation for a multiple flywheel system in variable configurations. *J. Vib. Control* **2015**, *21*, 105–123. [[CrossRef](#)]
76. Wan, Q.; Liu, G.; Shi, H.; Zhang, X.; Ning, X. Analysis of dynamic characteristics for momentum wheel assembly with joint clearance. *Adv. Mech. Eng.* **2018**, *10*, 1687814018818919. [[CrossRef](#)]
77. Chou, M.; Liaw, C. Dynamic control and diagnostic friction estimation for an SPMSM-driven satellite reaction wheel. *IEEE Trans. Ind. Electron.* **2011**, *58*, 4693–4707. [[CrossRef](#)]
78. Alcorn, J.; Allard, C.; Schaub, H. Fully coupled reaction wheel static and dynamic imbalance for spacecraft jitter modeling. *J. Guid. Control Dyn.* **2018**, *41*, 1380–1388. [[CrossRef](#)]
79. Wang, H.; Chen, L.; Jin, Z.; Crassidis, J. Adaptive momentum distribution jitter control for microsatellite. *J. Guid. Control Dyn.* **2019**, *42*, 632–641. [[CrossRef](#)]
80. Aghalari, A.; Shahravi, M. Nonlinear electromechanical modelling and dynamical behavior analysis of a satellite reaction wheel. *Acta Astronaut.* **2017**, *141*, 143–157. [[CrossRef](#)]
81. Narayan, S.; Nair, P.; Ghosal, A. Dynamic interaction of rotating momentum wheels with spacecraft element. *J. Sound Vib.* **2008**, *315*, 970–984. [[CrossRef](#)]
82. Wei, Z.; Li, D.; Luo, Q.; Jiang, J. Modeling and analysis of a flywheel microvibration isolation system for spacecrafts. *Adv. Space Res.* **2015**, *55*, 761–777. [[CrossRef](#)]
83. Preda, V.; Cieslak, J.; Henry, D.; Bennani, S.; Falcoz, A. A H1/ μ solution for microvibration mitigation in satellites: A case study. *J. Sound Vib.* **2017**, *399*, 21–44. [[CrossRef](#)]
84. Preda, V.; Cieslak, J.; Henry, D.; Bennani, S.; Falcoz, A. Robust microvibration mitigation and pointing performance analysis for high stability spacecraft. *Int. J. Robust Nonlinear Control* **2018**, *28*, 5688–5716. [[CrossRef](#)]
85. Zhou, W.; Li, D.; Lu, Q.; Liu, K. Analysis and testing of microvibrations produced by momentum wheel assemblies. *Chin. J. Aeronaut.* **2012**, *25*, 640–649. [[CrossRef](#)]
86. Han, Q.; Li, X.; Chu, F. Skidding behavior of cylindrical roller bearings under time-variable load conditions. *Int. J. Mech. Sci.* **2018**, *135*, 203–214. [[CrossRef](#)]
87. Wang, H.; Han, Q.; Zhou, D. Nonlinear dynamic modeling of rotor system supported by angular contact ball bearings. *Mech. Syst. Signal Process.* **2017**, *85*, 16–40. [[CrossRef](#)]
88. Wang, H.; Han, Q.; Luo, R.; Qing, T. Dynamic modeling of moment wheel assemblies with nonlinear rolling bearing supports. *J. Sound Vib.* **2017**, *406*, 124–145. [[CrossRef](#)]
89. Tang, L.; Xu, S. Geometric analysis of singularity for single-gimbal control moment gyro systems. *Chin. J. Aeronaut.* **2005**, *18*, 295–303. [[CrossRef](#)]
90. Zhang, J.; Jin, L.; Liu, Z. An improved installation for control moment gyros and its applications on reconfiguration and singular escape. *Acta Astronaut.* **2012**, *85*, 93–99.
91. Huang, X.; Jia, Y.; Xu, S.; Huang, T. A new steering approach for VSCMGs with high precision. *Chin. J. Aeronaut.* **2016**, *29*, 1673–1684. [[CrossRef](#)]
92. Wu, Z.; Zhang, J. Dynamics and control of gimbal servo systems for control moment gyroscopes. *J. Basic Sci. Eng.* **2007**, *15*, 130–136.
93. Huang, Z.; Li, X.; Jin, D. Output characteristic analysis of single gimbal control moment gyroscope. *Chin. J. Theor. Appl. Mech.* **2021**, *53*, 511–523.
94. Cui, P.; Zhang, D.; Yang, S.; Li, H. Friction compensation based on time-delay control and internal model control for a gimbal system in magnetically suspended CMG. *IEEE Trans. Ind. Electron.* **2017**, *64*, 3798–3807. [[CrossRef](#)]
95. Luo, Q.; Li, D.; Zhou, W.; Jiang, J.; Yang, G.; Wei, X. Dynamic modelling and observation of micro-vibrations generated by a single gimbal control moment gyro. *J. Sound Vib.* **2013**, *332*, 4496–4516. [[CrossRef](#)]
96. Luo, Q.; Li, D.; Jiang, J. Coupled dynamic analysis of a single gimbal control moment gyro cluster integrated with an isolation system. *J. Sound Vib.* **2014**, *333*, 345–363. [[CrossRef](#)]
97. Shi, S.; Li, D.; Luo, Q. Design and dynamic analysis of micro-vibration isolator for Single Gimbal Control Moment Gyro. *Procedia Eng.* **2015**, *99*, 551–559. [[CrossRef](#)]
98. Li, X.; Cheng, W.; Li, X. Modelling of gimbal control moment gyro and analysis of gimbal disturbance impact. *Teh. Vjesn.* **2014**, *21*, 1189–1199.
99. Li, X.; Cheng, W. Research on microvibrations generated by a control moment gyroscope on a flexible interface based on a dynamic substructure method. *Int. J. Aerosp. Eng.* **2018**, *2018*, 5045740. [[CrossRef](#)]

100. Wu, D.; Xie, T.; Lu, M.; Li, G.; Lai, L.; Yang, Y.; Wang, H. Modeling and experimental study on the micro-vibration transmission of a control moment gyro. *IEEE Access* **2019**, *7*, 80633–80643. [[CrossRef](#)]
101. Zhang, Y.; Zhang, J. Disturbance characteristics analysis of CMG due to imbalances and installation errors. *IEEE Trans. Aerosp. Electron. Syst.* **2014**, *50*, 1017–1026. [[CrossRef](#)]
102. Zhang, J.; Guo, Z.; Zhang, Y.; Tang, L.; Guan, X. Inner structural vibration isolation method for a single control moment gyroscope. *J. Sound Vib.* **2016**, *361*, 78–98. [[CrossRef](#)]
103. Wang, H.; Han, Q.; Zhou, D. Output torque modeling of control moment gyros considering rolling element bearing induced disturbances. *Mech. Syst. Signal Process.* **2019**, *115*, 188–212. [[CrossRef](#)]
104. Liu, K.C.; Maghami, P.; Blaurock, C. Reaction wheel disturbance modeling, jitter analysis, and validation tests for solar dynamics observatory. In Proceedings of the AIAA Guidance, Navigation and Control Conference and Exhibit, Honolulu, HI, USA, 19 August 2008; pp. 1–18.
105. Park, G.; Lee, D.; Han, J. Development of multi-degree-of-freedom microvibration emulator for efficient jitter test of spacecraft. *J. Intell. Mater. Syst. Struct.* **2014**, *25*, 1069–1081. [[CrossRef](#)]
106. Kim, D. Micro-vibration model and parameter estimation method of a reaction wheel assembly. *J. Sound Vib.* **2014**, *333*, 4214–4231. [[CrossRef](#)]
107. Sanfedino, F.; Alazard, D.; Pommier-Budinger, V.; Boquet, F.; Falcoz, A. A novel dynamic model of a reaction wheel assembly for high accuracy pointing space missions. In Proceedings of the ASME Dynamic Systems and Control Conference (DSCC-2018), Atlanta, GA, USA, 30 September–3 October 2018.
108. Lellis, S.; Stabile, A.; Aglietti, G.; Richardson, G. A semiempirical methodology to characterise a family of microvibration sources. *J. Sound Vib.* **2019**, *448*, 1–18. [[CrossRef](#)]
109. Hur, G.; Kim, K. Parametric vibration source characterization of a reaction-wheel-assembly by evaluation on predictions of blocked forces and simple receiver responses. *J. Mech. Sci. Technol.* **2018**, *32*, 4433–4445. [[CrossRef](#)]
110. Hur, G. Isolation of micro-vibrations due to reaction wheel assembly using a source-path-receiver approach for quantitative requirements. *J. Vib. Control* **2019**, *25*, 1424–1435. [[CrossRef](#)]
111. Hasha, M. High-performance reaction wheel optimization for fine-pointing space platforms: Minimizing induced vibration effects on jitter performance plus lessons learned from hubble space telescope for current and future spacecraft applications. In Proceedings of the 43rd Aerospace Mechanisms Symposium, NASA Ames Research Center, Santa Clara, CA, USA, 4–6 May 2016.
112. Inamori, T.; Wang, J.; Saisutjarit, P.; Nakasuka, S. Jitter reduction of a reaction wheel by management of angular momentum using magnetic torquers in nano- and micro-satellites. *Adv. Space Res.* **2013**, *52*, 222–231. [[CrossRef](#)]
113. Kim, D.; Yoon, H.; Kang, W.; Kim, Y.; Choi, H. Development of a spherical reaction wheel actuator using electromagnetic induction. *Aerosp. Sci. Technol.* **2014**, *39*, 86–94. [[CrossRef](#)]
114. Nagabhushan, V.; Fitz-Coy, N. On-orbit jitter control in momentum actuators using a three-flywheel system. *Acta Astronaut.* **2014**, *95*, 61–81. [[CrossRef](#)]
115. Rodrigues, D.; Champneys, A.; Friswell, M.; Wilson, R. Automatic two-plane balancing for rigid rotors. *Int. J. Non-Linear Mech.* **2008**, *43*, 527–541. [[CrossRef](#)]
116. Liu, J.; Ishida, Y. Vibration suppression of rotating machinery utilizing an automatic ball balancer and discontinuous spring characteristics. *ASME J. Vib. Acoust.* **2009**, *131*, 041004. [[CrossRef](#)]
117. Horvath, R.; Flowers, G.; Fausz, J. Passive balancing of rotor systems using pendulum balancers. *ASME J. Vib. Acoust.* **2008**, *130*, 041011. [[CrossRef](#)]
118. Mayr, J.; Spanlang, F.; Gattringer, H. Mechatronic design of a self-balancing three-dimensional inertia wheel pendulum. *Mechatronics* **2015**, *30*, 1–10. [[CrossRef](#)]
119. Chen, H.; Ji, W.; Zhang, Q. A method for vibration isolation of a vertical axis automatic washing machine with a hydraulic balancer. *J. Mech. Sci. Technol.* **2012**, *26*, 335–343. [[CrossRef](#)]
120. Cho, J.; Jeong, H.; Kong, K. Analysis of dynamic model of a top loading laundry machine with a hydraulic balancer. *Int. J. Precis. Eng. Manuf.* **2014**, *15*, 1615–1623. [[CrossRef](#)]
121. Zeng, S.; Wang, X. The influence of the electromagnetic balancing regulator on the rotor system. *J. Sound Vib.* **1999**, *219*, 723–729. [[CrossRef](#)]
122. Ma, S.; Pei, S.; Wang, L.; Xu, H. A novel active online electromagnetic balancing method: Principle and structure analysis. *ASME J. Vib. Acoust.* **2012**, *134*, 034503. [[CrossRef](#)]
123. Hredzak, B.; Guo, G. New electromechanical balancing device for active imbalance compensation. *J. Sound Vib.* **2006**, *294*, 737–751. [[CrossRef](#)]
124. Pan, X.; Wu, H.; Gao, J.; Wang, W. New liquid transfer active balancing system using compressed air for grinding machine. *ASME J. Vib. Acoust.* **2015**, *137*, 011002.
125. Zhang, X.; Liu, X.; Zhao, H. New active online balancing method for grinding wheel using liquid injection and free dripping. *ASME J. Vib. Acoust.* **2018**, *140*, 031001. [[CrossRef](#)]
126. Kawak, B. Development of a low-cost, low micro-vibration CMG for small agile satellite applications. *Acta Astronaut.* **2017**, *131*, 113–122. [[CrossRef](#)]
127. Huang, X.; Su, Z.; Wang, S.; Wei, X.; Wang, Y.; Hua, H. High-frequency disturbance force suppression mechanism of a flywheel equipped with a flexible dynamic vibration absorber. *J. Sound Vib.* **2020**, *26*, 2113–2124. [[CrossRef](#)]

128. Jacobs, J.; Meffe, M.; Hightower, R. Piezodynamic Vibration Damping System. WIPO Patent WO/2005/002967, 13 January 2005.
129. Meffe, M.; Hightower, R.; Jacobs, J. Piezodynamic Preload Adjustment System. WIPO Patent WO/2005/003579A1, 30 December 2005.
130. Hindle, T.; Davis, T.; Hamilton, B.; Winkel, R. Vibration Reduction System Employing Active Bearing Mounts. U.S. Patent 8002251, 23 August 2003.
131. Xie, Y.; Sawada, H.; Hashimoto, T. Adaptive model following control method for actively controlled magnetic bearing momentum wheel. In Proceedings of the 5th International Symposium on Magnetic Suspension Technology, Santa Barbara, CA, USA, 11–13 December 1999; pp. 547–561.
132. Xie, J.; Liu, G.; Wen, T. Composite compensation for load torque of active magnetic bearing in DGMSCMG. *Opt. Precis. Eng.* **2015**, *23*, 2211–2219.
133. Cui, P.; Gai, Y.; Fang, J. Adaptive control for unbalance vibration of active-passive hybrid magnetically suspended rotor. *Opt. Precis. Eng.* **2015**, *23*, 122–131.
134. Kaufmann, M.; Tuysuz, A.; Kolar, J.; Zwyssig, C. High-speed magnetically levitated reaction wheels for small satellites. In Proceedings of the 23rd International Symposium on Power Electronics, Electrical Drives, Automation and Motion (SPEEDAM 2016), Anacapri, Italy, 22–24 June 2016.
135. Liu, G.; Zhang, C. Sliding mode control of reaction flywheel-based brushless DC motor with buck converter. *Chin. J. Aeronaut.* **2013**, *26*, 967–975. [[CrossRef](#)]
136. Liu, Q.; Wang, K.; Ren, Y. Novel repeatable launch locking/unlocking device for magnetically suspended momentum flywheel. *Mechatronics* **2018**, *54*, 16–25.
137. Tang, J.; Fang, J.; Wen, T. Superconducting magnetic bearings and active magnetic bearings in attitude control and energy storage flywheel for spacecraft. *IEEE Trans. Appl. Supercond.* **2012**, *22*, 5702109. [[CrossRef](#)]
138. Liu, Q.; Zhao, M.; Han, B.; Zhang, J.; Sun, J.; Fan, Y. Research and development status of magnetic bearing technology on magnetically suspended gimballed flywheel. *J. Astronaut.* **2019**, *40*, 1251–1261.
139. Bichler, U. A low noise magnetic bearing wheel for space application. In Proceedings of the 2nd International Symposium on Magnetic Bearing, Tokyo, Japan, 12–14 July 1990; pp. 1–8.
140. Liu, B.; Fang, J.; Liu, G.; Fan, Y. Unbalance vibration control and experiment research of magnetically suspended flywheels. *J. Mech. Eng.* **2010**, *46*, 188–194. [[CrossRef](#)]
141. Tang, J.; Liu, B.; Fang, J.; Ge, S. Suppression of vibration caused by residual unbalance of rotor for magnetically suspended flywheel. *J. Vib. Control* **2012**, *19*, 1962–1979. [[CrossRef](#)]
142. Xu, X.; Chen, S.; Zhang, Y. Automatic balancing of AMB systems using plural notch filter and adaptive synchronous compensation. *J. Sound Vib.* **2016**, *374*, 29–42. [[CrossRef](#)]
143. Peng, C.; Fan, Y.; Huang, Z.; Han, B.; Fang, J. Frequency-varying synchronous micro-vibration suppression for a MSFW with application of small-gain theorem. *Mech. Syst. Signal Process.* **2017**, *82*, 432–447. [[CrossRef](#)]
144. Peng, C.; Zhou, X.; Wei, T.; Ren, Y. High precision synchronous vibration suppression for a MSFW subject to phase lag influence. *Mech. Syst. Signal Process.* **2019**, *120*, 408–421. [[CrossRef](#)]
145. Basaran, S.; Sivrioglu, S.; Zergeroglu, E. Composite adaptive control of single gimbal control moment gyroscope supported by active magnetic bearings. *ASCE J. Aerosp. Eng.* **2016**, *30*, 04016074. [[CrossRef](#)]
146. Tang, J.; Zhao, S.; Wang, Y.; Wang, K. High-speed rotor's mechanical design and stable suspension based on inertia-ratio for gyroscopic effect suppression. *Int. J. Control Autom. Syst.* **2018**, *16*, 1577–1591. [[CrossRef](#)]
147. Deng, R.; Zhao, Y.; Fang, J.; Zhang, D. Disturbance characteristics analysis of magnetically suspended and mechanical flywheels. *J. Astronaut.* **2016**, *37*, 917–923.
148. Liu, C.; Jing, X.; Daley, S.; Li, F. Recent advances in micro-vibration isolation. *Mech. Syst. Signal Process.* **2015**, *56–57*, 55–80. [[CrossRef](#)]
149. Kamesh, D.; Pandiyan, R.; Ghosal, A. Passive vibration isolation of reaction wheel disturbances using a low frequency flexible space platform. *J. Sound Vib.* **2012**, *331*, 1310–1330. [[CrossRef](#)]
150. Kamesh, D.; Pandiyan, R.; Ghosal, A. Modeling, design and analysis of low frequency platform for attenuating micro-vibration in spacecraft. *J. Sound Vib.* **2010**, *329*, 3431–3450. [[CrossRef](#)]
151. Zhou, W.Y.; Li, D.X. Design and analysis of an intelligent vibration isolation platform for reaction/momentum wheel assemblies. *J. Sound Vib.* **2012**, *331*, 2984–3005. [[CrossRef](#)]
152. Zhou, W.; Li, D. Experimental research on a vibration isolation platform for momentum wheel assembly. *J. Sound Vib.* **2013**, *332*, 1157–1171. [[CrossRef](#)]
153. Wei, Z.; Li, D.; Luo, Q.; Jiang, J. Performance analysis of a flywheel microvibration isolation platform for spacecraft. *J. Spacecr. Rocket.* **2015**, *52*, 1263–1268. [[CrossRef](#)]
154. Luo, Y.; Zhang, Y.; Zhang, X.; Gao, X.; Jia, K.; Xu, M. Modeling and analysis of piezoelectric folded-beam isolator for attenuating micro-vibration in spacecraft. *Int. J. Comput. Mater. Sci. Eng.* **2018**, *7*, 1850013. [[CrossRef](#)]
155. Dong, G.; Zhang, X.; Xie, S.; Yan, B.; Luo, Y. Simulated and experimental studies on a high-static-low-dynamic stiffness isolator using magnetic negative stiffness spring. *Mech. Syst. Signal Process.* **2017**, *86*, 188–203. [[CrossRef](#)]
156. Zhang, Q.; Wang, G.; Zheng, G. Micro-vibration attenuation methods and key technologies for optical remote sensing satellite. *J. Astronaut.* **2015**, *36*, 125–132.

157. Jiao, X.; Zhao, Y.; Ma, W. Nonlinear dynamic characteristics of a micro-vibration fluid viscous damper. *Nonlinear Dyn.* **2018**, *92*, 1167–1184. [[CrossRef](#)]
158. Rodden, J.; Dougherty, H.; Reschke, L. Line-of-sight performance improvement with reaction-wheel isolation. In *Proceeding of the Annual Rocky Mountain Guidance and Control Conference*, Keytone, CO, USA, 1–5 February 1986; pp. 71–84.
159. Wang, X.; Zheng, G. Two-step transfer function calculation method and asymmetrical piecewise-linear vibration isolator under gravity. *J. Vib. Control* **2016**, *22*, 2973–2991. [[CrossRef](#)]
160. Kwon, S.; Jo, M.; Oh, H. Experimental validation of fly-wheel passive launch and on-orbit vibration isolation system by using a superelastic SMA mesh washer isolator. *Int. J. Aerosp. Eng.* **2017**, *2017*, 5496053. [[CrossRef](#)]
161. Li, L.; Tan, L.; Kong, L.; Wang, D.; Yang, H. The influence of flywheel micro vibration on space camera and vibration suppression. *Mech. Syst. Signal Process.* **2018**, *100*, 360–370. [[CrossRef](#)]
162. Chen, S.; Xuan, M.; Xin, J.; Liu, Y.; Gu, S.; Li, J.; Zhang, L. Design and experiment of dual micro-vibration isolation system for optical satellite flywheel. *Int. J. Mech. Sci.* **2020**, *179*, 105592. [[CrossRef](#)]
163. Oh, H.; Taniwaki, S.; Kinjyo, N.; Izawa, K. Flywheel vibration isolation test using a variable-damping isolator. *Smart Mater. Struct.* **2006**, *15*, 365–370. [[CrossRef](#)]
164. Magliacano, D.; Viscardi, M.; Dimino, I. Active vibration control by piezoceramic actuators of a car floor panel. In *Proceedings of the 23rd International Congress on Sound and Vibration (ICSV23)*, Athens, Greece, 10–14 July 2016.
165. Makiyama, K.; Onoda, J.; Minesugi, K. New approach to semi-active vibration isolation to improve the pointing performance of observation satellites. *Smart Mater. Struct.* **2006**, *15*, 342–350. [[CrossRef](#)]
166. Zhang, Y.; Chen, Z.; Jiao, Y. A hybrid vibration isolator: Design, control, and experiments. *Proc. IMechE C J. Mech. Eng. Sci.* **2016**, *230*, 2982–2995. [[CrossRef](#)]
167. Wang, C.; Chen, Y.; Zhang, Z. Simulation and experiment on the performance of a passive/active micro-vibration isolator. *J. Vib. Control* **2018**, *24*, 453–465. [[CrossRef](#)]
168. Guan, X.; Cui, Y.; Liang, L.; Zheng, G. Development and experimental verification of flywheel vibration isolation device. In *Proceeding of the Structural Vibration and Control Technology for High Resolution Remote Sensing Satellites*, Changsha, China, 10–14 July 2011; pp. 38–44.
169. Zhao, W.; Li, B.; Liu, P. Semi-active control for a multi-dimensional vibration isolator with parallel mechanism. *J. Vib. Control* **2012**, *19*, 879–888. [[CrossRef](#)]
170. Lee, D.; Park, G.; Han, J. Experimental study on on-orbit and launch environment vibration isolation performance of a vibration isolator using bellows and viscous fluid. *Aerosp. Sci. Technol.* **2015**, *45*, 1–9. [[CrossRef](#)]
171. Li, Y.; Yun, Y.; Xiao, S. Controller design and experimental investigation of a 3-universal-prismatic-universal compliant manipulator for active vibration isolation. *J. Vib. Control* **2015**, *21*, 3218–3238. [[CrossRef](#)]
172. Kim, H.; Cho, Y.; Moon, J. Active vibration control using a novel three-DOF precision micro-stage. *Smart Mater. Struct.* **2010**, *19*, 055001. [[CrossRef](#)]
173. Xu, Z.; Xu, F.; Chen, X. Vibration suppression on a platform by using vibration isolation and mitigation devices. *Nonlinear Dyn.* **2016**, *83*, 1341–1353. [[CrossRef](#)]
174. Xu, C.; Xu, Z.; Huang, Y.; Xu, Y.; Ge, T. Modeling and analysis of a viscoelastic micro-vibration isolation and mitigation platform for spacecraft. *J. Vib. Control* **2018**, *24*, 4337–4352. [[CrossRef](#)]
175. Xu, Z.; Xu, F.; Chen, X. Intelligent vibration isolation and mitigation of a platform by using MR and VE devices. *J. Aerosp. Eng.* **2016**, *29*, 04016010. [[CrossRef](#)]
176. Spanos, J.; Rahman, Z.; Blackwood, G. A soft-axis active vibration isolator. In *Proceedings of the American Control Conference*, Seattle, WA, USA, 21–23 June 1995; pp. 412–416.
177. Dasgupta, B.; Mruthyunjaya, T. The Stewart platform manipulator: A review. *Mech. Mach. Theory* **2000**, *35*, 15–40. [[CrossRef](#)]
178. Preumont, A.; Horodincu, M.; Romanescu, I.; Marneffe, B.; Avraam, M.; Deraemaeker, A.; Bossens, F.; Hanieh, A. A six-axis single-stage active vibration isolator based on Stewart platform. *J. Sound Vib.* **2007**, *300*, 644–661. [[CrossRef](#)]
179. Pendergast, K.; Schauwecker, C. Use of a passive reaction wheel jitter isolation system to meet the advanced X-ray astrophysics facility imaging performance requirements. In *Proceedings of the SPIE Conference on Space Telescopes and Instruments V*, Kona, HI, USA, 20 March 1998; Volume 3356, pp. 1078–1094.
180. Lee, D.; Park, G.; Han, J.H. Hybrid isolation of micro vibrations induced by reaction wheels. *J. Sound Vib.* **2016**, *363*, 1–17. [[CrossRef](#)]
181. Yang, X.; Wu, H.; Li, Y.; Chen, B. Dynamic isotropic design and decentralized active control of a six-axis vibration isolator via Stewart platform. *Mech. Mach. Theory* **2017**, *117*, 244–252. [[CrossRef](#)]
182. Yang, X.; Wu, H.; Chen, B.; Kang, S.; Cheng, S. Dynamic modeling and decoupled control of a flexible Stewart platform for vibration isolation. *J. Sound Vib.* **2019**, *439*, 398–412. [[CrossRef](#)]
183. Qin, C.; Xu, Z.; Xia, M.; He, S.; Zhang, J. Design and optimization of the micro-vibration isolation system for large space telescope. *J. Sound Vib.* **2020**, *482*, 115461. [[CrossRef](#)]
184. Wu, Y.; Yu, K.; Jiao, J.; Zhao, R. Dynamic modeling and robust nonlinear control of a six-DOF active micro-vibration isolation manipulator with parameter uncertainties. *Mech. Mach. Theory* **2015**, *92*, 407–435. [[CrossRef](#)]
185. Wu, Y.; Yu, K.; Jiao, J.; Cao, D.; Chi, W.; Tang, J. Dynamic isotropy design and analysis of a six-DOF active micro-vibration isolation manipulator on satellites. *Robot. Comput.-Integr. Manuf.* **2018**, *49*, 408–425. [[CrossRef](#)]

186. Hauge, G.; Campbell, M. Sensors and control of a space-based six-axis vibration isolation system. *J. Sound Vib.* **2004**, *269*, 913–931. [[CrossRef](#)]
187. Anderson, E.; Fumo, J.; Erwin, R. Satellite ultra-quiet isolation technology experiment (SUITE). In Proceedings of the IEEE Aerospace Conference, Piscataway, NJ, USA, 25 March 2000; pp. 299–313.
188. Wang, C.; Xie, X.; Chen, Y.; Zhang, Z. Investigation on active vibration isolation of a Stewart platform with piezoelectric actuators. *J. Sound Vib.* **2016**, *383*, 1–19. [[CrossRef](#)]
189. Yun, H.; Liu, L.; Li, Q.; Yang, H. Investigation on two-stage vibration suppression and precision pointing for space optical payloads. *Aerosp. Sci. Technol.* **2020**, *96*, 105543. [[CrossRef](#)]
190. Sun, X.; Yang, B.; Zhao, L.; Sun, X. Optimal design and experimental analyses of a new micro-vibration control payload-platform. *J. Sound Vib.* **2016**, *374*, 43–60. [[CrossRef](#)]
191. Thayer, D.; Campbell, M.; Vagners, J. Six-axis vibration isolation system using soft actuators and multiple sensors. *J. Spacecr. Rocket.* **2002**, *39*, 206–212. [[CrossRef](#)]
192. Beijen, M.; Heertjes, M.; Dijk, J.; Hakvoort, W. Self-tuning MIMO disturbance feedforward control for active hard-mounted vibration isolators. *Control Eng. Pract.* **2018**, *72*, 90–103. [[CrossRef](#)]
193. Zhang, Y.; Sheng, C.; Hu, Q.; Li, M.; Guo, Z.; Qi, R. Dynamic analysis and control application of vibration isolation system with magnetic suspension on satellites. *Aerosp. Sci. Technol.* **2018**, *75*, 99–114. [[CrossRef](#)]
194. Guo, Z.; Zhang, Y.; Hu, Q. Integrated vibration isolation and attitude control for spacecraft with uncertain or unknown payload inertia parameters. *Acta Astronaut.* **2018**, *151*, 107–119. [[CrossRef](#)]
195. Zhang, Y.; Xu, S. Vibration isolation platform for control moment gyroscopes on satellites. *J. Aerosp. Eng.* **2012**, *25*, 641–652. [[CrossRef](#)]
196. Zhang, Y.; Guo, Z.; He, H.; Zhang, J.; Liu, M.; Zhou, Z. A novel vibration isolation system for reaction wheel on space telescopes. *Acta Astronaut.* **2014**, *102*, 1–13. [[CrossRef](#)]
197. Zhang, Y.; Zhang, J. The imaging stability enhancement of optical payload using multiple vibration isolation platforms. *J. Vib. Control* **2015**, *21*, 1848–1865.
198. Zhang, Y.; Zang, Y.; Li, M.; Wang, Y.; Li, W. Active-passive integrated vibration control for control moment gyros and its application to satellites. *J. Sound Vib.* **2017**, *394*, 1–14. [[CrossRef](#)]
199. Zhang, Y.; Sheng, C.; Guo, Z.; Wang, Y.; Li, W. Dynamic characteristics and performance evaluation for the part strut failure of the vibration isolation platform on satellites. *Acta Astronaut.* **2017**, *133*, 403–415. [[CrossRef](#)]
200. Heiberg, C.; Bailey, D.; Wie, B. Precision spacecraft pointing using single-gimbal control moment gyroscopes with disturbance. *J. Guid. Control Dyn.* **2000**, *23*, 77–85. [[CrossRef](#)]
201. Huang, X.; Sun, J.; Hua, H.; Zhang, Z. Modeling and optimization of octostrut vibration isolation platform by FRF-based substructuring method. *J. Aerosp. Eng.* **2015**, *28*, 04014084. [[CrossRef](#)]
202. Luo, Q.; Li, D.; Jiang, J. Analysis and optimization of micro-vibration isolation for multiple flywheel systems of spacecraft. *AIAA J.* **2016**, *54*, 1719–1731. [[CrossRef](#)]
203. Wu, Q.; Yue, H.; Liu, R.; Zhang, X.; Ding, L.; Liang, T.; Deng, Z. Measurement model and precision analysis of accelerometers for maglev vibration isolation platforms. *Sensors* **2015**, *15*, 20053–20068. [[CrossRef](#)] [[PubMed](#)]
204. Gong, Z.; Ding, L.; Yue, H.; Gao, H.; Liu, R.; Deng, Z.; Lu, Y. System integration and control design of a maglev platform for space vibration isolation. *J. Vib. Control* **2019**, *25*, 1720–1736. [[CrossRef](#)]
205. Gong, Z.; Ding, L.; Li, S.; Yue, H.; Gao, H.; Deng, Z. Payload-agnostic decoupling and hybrid vibration isolation control for a maglev platform with redundant actuation. *Mech. Syst. Signal Process.* **2021**, *146*, 106985. [[CrossRef](#)]
206. Xiao, X.; Jing, X.; Cheng, L. The transmissibility of vibration isolators with cubic nonlinear damping under both force and base excitations. *J. Sound Vib.* **2013**, *332*, 1335–1354. [[CrossRef](#)]
207. Sun, J.; Huang, X.; Liu, X.; Xiao, F.; Huang, H. Study on the force transmissibility of vibration isolators with geometric nonlinear damping. *Nonlinear Dyn.* **2013**, *74*, 1103–1112. [[CrossRef](#)]
208. Yan, B.; Ma, H.; Zheng, W.; Jian, B.; Wang, K.; Wu, C. Nonlinear electromagnetic shunt damping for nonlinear vibration isolators. *IEEE/ASME Trans. Mechatron.* **2019**, *24*, 1851–1860. [[CrossRef](#)]
209. Yan, B.; Ma, H.; Zhang, L.; Zheng, W.; Wang, K.; Wu, C. A bistable vibration isolator with nonlinear electromagnetic shunt damping. *Mech. Syst. Signal Process.* **2020**, *136*, 106504. [[CrossRef](#)]
210. Ma, H.; Yan, B. Nonlinear damping and mass effects of electromagnetic shunt damping for enhanced nonlinear vibration isolation. *Mech. Syst. Signal Process.* **2021**, *146*, 107010. [[CrossRef](#)]
211. Stabile, A.; Aglietti, G.; Richardson, G.; Smet, G. Design and verification of a negative resistance electromagnetic shunt damper for spacecraft micro-vibration. *J. Sound Vib.* **2017**, *386*, 38–49. [[CrossRef](#)]
212. Stabile, A.; Aglietti, G.; Richardson, G.; Smet, G. A 2-collinear-DoF strut with embedded negative-resistance electromagnetic shunt dampers for spacecraft micro-vibration. *Smart Mater. Struct.* **2017**, *26*, 045031. [[CrossRef](#)]
213. Zhou, J.; Xiao, Q.; Xu, D.; Ouyang, H.; Li, Y. A novel quasi-zero-stiffness strut and its applications in six-degree-of-freedom vibration isolation platform. *J. Sound Vib.* **2017**, *394*, 59–74. [[CrossRef](#)]
214. Zheng, Y.; Li, Q.; Yan, B.; Luo, Y.; Zhang, X. A Stewart isolator with high-static-low-dynamic stiffness struts based on negative stiffness magnetic springs. *J. Sound Vib.* **2018**, *422*, 390–408. [[CrossRef](#)]

215. Dong, G.; Zhang, X.; Luo, Y.; Zhang, Y.; Xie, S. Analytical study of the low frequency multi-direction isolator with high-static-low-dynamic stiffness struts and spatial pendulum. *Mech. Syst. Signal Process.* **2018**, *110*, 521–539. [[CrossRef](#)]
216. Palomares, E.; Nieto, A.; Moreales, A.; Chicharro, J.; Pintado, P. Numerical and experimental analysis of a vibration isolator equipped with a negative stiffness system. *J. Sound Vib.* **2018**, *414*, 31–42. [[CrossRef](#)]
217. Liu, C.; Jing, X.; Li, F. Vibration isolation using a hybrid lever-type isolation system with an X-shape supporting structure. *Int. J. Mech. Sci.* **2015**, *98*, 169–177. [[CrossRef](#)]
218. Wang, Y.; Jing, X.; Guo, Y. Nonlinear analysis of a bio-inspired vertically asymmetric isolation system under different structural constraints. *Nonlinear Dyn.* **2019**, *95*, 445–464. [[CrossRef](#)]
219. Wang, Y.; Jing, X. Nonlinear stiffness and dynamical response characteristics of an asymmetric X-shaped structure. *Mech. Syst. Signal Process.* **2019**, *125*, 142–169. [[CrossRef](#)]
220. Sun, M.; Song, G.; Li, Y.; Huang, Z. Effect of negative stiffness mechanism in a vibration isolator with asymmetric and high-static-low-dynamic stiffness. *Mech. Syst. Signal Process.* **2019**, *124*, 388–407. [[CrossRef](#)]
221. Yang, G.; Zou, H.; Wang, S.; Zhao, L.; Gao, Q.; Tan, T.; Zhang, W. Large stroke quasi-zero stiffness vibration isolator using three-link mechanism. *J. Sound Vib.* **2020**, *478*, 115344.
222. Liu, H.; Wang, Y.; Shi, W. Vibration suppression for a flywheel based on nonlinear energy sink. *J. Astronaut.* **2017**, *38*, 490–496.
223. Sun, Y.; Zhang, Y.; Ding, H.; Chen, L. Nonlinear energy sink for a flywheel system vibration reduction. *J. Sound Vib.* **2018**, *429*, 305–324. [[CrossRef](#)]
224. Sun, X.; Zhang, S.; Xu, J. Parameter design of a multi-delayed isolator with asymmetrical nonlinearity. *Int. J. Mech. Sci.* **2018**, *138–139*, 398–408. [[CrossRef](#)]
225. Chen, S.; Xuan, M.; Zhang, L.; Gu, S.; Gong, X.; Sun, H. Simulating and testing microvibrations on an optical satellite using acceleration sensor-based jitter measurements. *Sensors* **2019**, *19*, 1797. [[CrossRef](#)]
226. Chen, J.; Cheng, W. Low-frequency compensation of piezoelectric micro-vibrations test platform. *Teh. Vjesn.* **2016**, *23*, 1251–1258.
227. Xia, M.; Xu, Z.; Han, K.; Huo, Q.; Li, A. Dynamic disturbance force measurement platform for large moving device in spacecraft. *J. Sound Vib.* **2019**, *447*, 61–77. [[CrossRef](#)]
228. Elias, L. *A Structurally Coupled Disturbance Analysis Method Using Dynamic Mass Measurement Techniques, with Application to Spacecraft-Reaction Wheel Systems*; Massachusetts Institute of Technology: Cambridge, MA, USA, 2001.
229. Zhao, Y.; Zhang, P.; Cheng, W. Measurement and study of disturbance characteristics of reaction wheel assembly. *J. Exp. Mech.* **2009**, *24*, 532–538.
230. Taniwaki, S.; Kudo, M.; Sato, M. Analysis of retainer induced disturbances of reaction wheel. *J. Syst. Des. Dyn.* **2007**, *1*, 307–317. [[CrossRef](#)]
231. Taniwaki, S.; Hatsutori, Y.; Ohkami, Y. Development of lower frequency disturbance detector for reaction wheel analysis. In Proceedings of the ASME International Mechanical Engineering Congress and Exposition, Orlando, FL, USA, 5–11 November 2005. IMECE2005-79318.
232. Wang, X.; Xu, Z.; He, S.; Wu, Q.; Li, H.; Zhao, Y.; He, L. Modeling and analysis of a multi-degree-of-freedom micro-vibration simulator. *Shock Vib.* **2017**, *2017*, 4840514. [[CrossRef](#)]
233. Wang, X.; Xu, Z.; Xia, M.; He, S.; Li, H.; Wu, Q. Research on a six-degree-of-freedom disturbance force and moment simulator for space micro-vibration experiments. *J. Sound Vib.* **2018**, *432*, 530–548. [[CrossRef](#)]

Disclaimer/Publisher’s Note: The statements, opinions and data contained in all publications are solely those of the individual author(s) and contributor(s) and not of MDPI and/or the editor(s). MDPI and/or the editor(s) disclaim responsibility for any injury to people or property resulting from any ideas, methods, instructions or products referred to in the content.